Revision 1

The new mineral cuprozheshengite, $Pb_4CuZn_2(AsO_4)_2(PO_4)_2(OH)_2$, from Yunnan province, China, with site-selective As-P substitution

Ningyue Sun[1], Ian E. Grey[2], Guowu Li[1]*, Christian Rewitzer[3], Yuan Xue[1], William G. Mumme[2], Hongtao Shen[4,5], Jinhua Hao[1], Colin M. MacRae[2], Alan Riboldi-Tunnicliffe[6], Stephanie Boer[6], Tim Williams[7], Anthony R. Kampf [8]

[1]Science Research Institute, China University of Geosciences, 100083 Beijing, China

[2]CSIRO Mineral Resources, Private Bag 10, 3169 Clayton South, Victoria, Australia

[3]Stadtplatz 17, 93437 Furth im Wald, Germany

[4]School of Resources and Environmental Engineering, Wuhan University of Technology, 430070 Wuhan, China

[5]State Key Laboratory of Geological Processes and Mineral Resources, China University of Geosciences, 430074 Wuhan, China

[6]Australian Synchrotron, 800 Blackburn Road, 3168 Clayton, Victoria, Australia

[7]Monash Centre for Electron Microscopy, Monash University, 3800 Clayton, Victoria, Australia

[8]Mineral Sciences Department, Natural History Museum of Los Angeles County, 900 Exposition Boulevard, 90007 Los Angeles, CA, USA

*Corresponding author: Prof. Guowu Li (liguowu@cugb.edu.cn)

Word count:7801 words

ABSTRACT

Cuprozheshengite (IMA2021-095a), $Pb_4CuZn_2(AsO_4)_2(PO_4)_2(OH)_2$, is a new mineral species from Sanguozhuang Village and Laochang of Yunnan Province, China. It occurs as sub-mm greenish-blue hemispherical aggregates of microscopic blade-like crystals on hemimorphite and is closely associated with veszelyite and galena. Cuprozheshengite is brittle with irregular fracture, a Mohs hardness of 2½–3, and perfect cleavage on {011}. The calculated density is 5.91 g/cm^3. The empirical chemical formula of the holotype is $(Pb_{3.97}Na_{0.04}Ca_{0.01})_{\Sigma 4.02}Cu_{1.06}Zn_{2.09}(AsO_4)_2[(P_{0.84}As_{0.12}Si_{0.01})_{\Sigma 0.97}O_4]_2(OH)_2$ based on 18 O atoms per formula unit. Cuprozheshengite is triclinic, space group *P*-1(#2), with unit-cell parameters a = 4.7977(8), b = 8.5789(8), c = 10.3855(9) Å, α = 97.270(8)°, β = 101.902(12)°, γ = 91.495(11)°, V = 414.30(9) Å^3, and Z = 1. Cuprozheshengite is a member of dongchuanite group, whose general formula is $A_4{}^{VI}B^{IV}B_2(X1O_4)_2(X2O_4)_2(OH)_2$, where A is an interlayer cation with Pb being dominant; B are transition metals with two crystallographic positions, ${}^{IV}B$ has tetrahedral coordination and fully occupied by Zn, while ${}^{VI}B$ has octahedral coordination and dominated by Zn or Cu; $X1$ and $X2$ are cations with tetrahedral coordination, occupied by As and P. Like other dongchuanite group minerals, the structural framework of cuprozheshengite is composed of two heteropolyhedral columns along [100]. Type 1 columns are composed of corner-linked $[{}^{IV}BO_4]$ and $[X2O_4]$ tetrahedra. Each tetrahedron is 3-connected with other tetrahedra in the columns. Type 2 columns have alternating $[{}^{VI}BO_4(OH)_2]$ octahedra with pairs of

corner-connected [$X1O_4$] tetrahedra. These two columns are connected by corner-sharing between [$^{IV}BO_4$] and [$X1O_4$] tetrahedra to form layers parallel to (011). Pb atoms occupy two independent sites between the layers. Cuprozheshengite is named as the copper analogue of zheshengite. Single-crystal X-ray study reveals that As-P ordering separation in *X*1 and *X*2 sites and As tends to occupy the *X*1 site preferentially. The structural geometric parameters and density functional theory (DFT) calculation study of cuprozheshengite provide critical evidence for the occupancy propensity of As benefiting structural stability, which provides a new idea for studying other rare minerals with atoms ordering at different sites. Besides, the structure and stability studies of cuprozheshengite may have implications for local environmental governance. As a stable mineral in the water and elemental cycles after weathering, cuprozheshengite still has the potential to continually crystallize in the local area. By converting waste pollution into a crystalline form, humans can maintain favorable environmental conditions comparable to geological periods on Earth.

Keywords: cuprozheshengite, dongchuanite group, new mineral, crystal structure, DFT calculation, As-P ordering

INTRODUCTION

Cuprozheshengite (IMA2021-095a), $Pb_4CuZn_2(AsO_4)_2(PO_4)_2(OH)_2$, is a new mineral species from Dongchuan and Laochang deposits in Yunnan Province, China. Other three related isomorphous minerals, dongchuanite, cuprodongchuanite, and

zheshengite, have been approved by the Commission on New Minerals, Nomenclature and Classification of the International Mineralogical Association (IMA-CNMNC), and they constitute the dongchuanite group. Cuprozheshengite is the Cu analogue of zheshengite, $Pb_4ZnZn_2(AsO_4)_2(PO_4)_2(OH)_2$ (Li et al. 2022). Their general formula is $A_4^{VI}B^{IV}B_2(X1O_4)_2(X2O_4)_2(OH)_2$, where $X1$ and $X2$ are cations with tetrahedral coordination, occupied by As and P. Our study shows that cuprozheshengite is a typical example of a mineral with As-P atoms ordered distribution at $X1$ and $X2$ sites, which has an essential enlightenment for mineral classification.

As and P, having comparable chemical properties and a tetrahedral geometry, usually form solid solution series minerals (Bajda et al. 2011; Biagioni et al. 2016). To be noted, As and P are generally ordered when homophase substitutions occur at different structural sites. Specifically, just as philipsburgite, $Cu_5Zn[(AsO_4)(PO_4)](OH)_6\cdot H_2O$, is an intermediate member with PO_4/AsO_4 ordering, between kipushite, $Cu_5Zn[(PO_4)(PO_4)](OH)_6\cdot H_2O$ and goldhillite, $Cu_5Zn[(AsO_4)(AsO_4)](OH)_6\cdot H_2O$ (Ismagilova et al. 2022; Krivovichev et al. 2018). But this ordered distribution lacks systematic research and it is not clear whether it is a statistical coincidence caused by few samples (Ismagilova et al. 2022; Siidra et al. 2021; Yakovenchuk et al. 2017). This study's structural geometric parameters and density functional theory (DFT) calculation for cuprozheshengite provide critical evidence that this tendency benefits structural stability.

Moreover, the study of the structural stability of As-rich minerals is a key issue in arsenic pollution remediation, which is a global concerned ecological problem

(Rakovan and Pasteris 2015). Various natural (e.g., geothermal heating and mineral weathering) and anthropogenic (e.g., agriculture and mining) processes can contribute to elevated concentrations of As in freshwater (Kocourkova-Vikova et al. 2015; Kunhikrishnan et al. 2017; Liang et al. 2021). Regarding public health, As in water ranks among the most significant threats due to its biotoxicity and carcinogenic potential (Antelo et al. 2015). Accordingly, the World Health Organization (WHO) recommends an arsenic limit of 10 μg/L for drinking water (Xing et al. 2022). The Dongchuan Cu ore field ranks by area as the world's third or fourth-largest sediment-hosted strata-bound copper district (Hitzman et al. 2005; Zhao 2012). With intensive mining over the past decade, a large amount of ore has been artificially exposed. Minerals, mainly As-bearing sulfides, undergo weathering, allowing arsenic ions to dissociate and participate in the water cycle. The As content of surface water in the Dongchuan area ranges from 14 to 48 μg/L, which significantly increases the health risks to the population (Zhao and Yang 2022). Zheshengite and cuprozheshengite provide important insights into our understanding of As in the local water and element cycle. The preference incorporation of As^{5+} into specific crystallographic sites as $(AsO_4)^{3-}$ makes it possible to fix As into a stable crystalline structure even when the As concentration is relatively low. The structure and stability studies of cuprozheshengite may have implications for local environmental governance.

OCCURRENCE AND MINERAL DESCRIPTION

Occurrence

Cuprozheshengite from two localities was investigated: The Dongchuan sample (DC sample) (Fig. 2a) provided by one of the authors (S.N.) was found at the Sanguozhuang Village, Tangdan Town, Dongchuan District, Kunming City, Yunnan Province, China (26° 8' 14'' N, 102° 59' 36'' E). Another Laochang sample (LC sample) (Fig. 2b) found by the author (C.R.) was from the Laochang mine (23° N, 103° E) in the Gejiu base metal sulfide ore field, Gejiu City, Yunnan Province, China.

Sanguozhuang Village is located east of the Dongchuan Cu ore field, where sedimentary rock-hosted strata-bound copper deposits are widespread (Zhao et al. 2010; Ma et al. 2014). The deposits of this type contain disseminated and veinlet copper sulfides along a regional redox boundary above weakly metamorphosed hematitic sandstones and siltstones within a weakly metamorphosed (Zhao et al. 2012). The DC specimens were collected from an abandoned mine about 1.7 kilometers northwest of Sanguzhuang Village, where the altitude is over 3000 meters (Fig. 1a, 1b). The primary sulfide minerals forming veins are chalcopyrite, sphalerite, bornite, chalcocite, and tetrahedrite group minerals with minor pyrite, digenite, galena, and covellite (Fig. 1c). In sandstone fractures around Cu-sulphide ore veins (Fig. 1d), plentiful supergene minerals are found including theisite, veszelyite, hemimorphite, kipushite, bayldonite, arsendescloizite, duftite, arsenoveszelyite, dongchuantie, cuprodongchuanite, zheshengite, cuprozheshengite, etc. The type specimen of DC (Fig. 2a) shows that cuprozheshengite is closely associated with veszelyite and hemimorphite.

Samples from Laochang were found in a mineral collection sample present as light greenish-blue hemispheres on a hemimorphite matrix (Fig. 2b). Other associated minerals are veszelyite, theisite, and galena. The Laochang deposit is an important part of Gejiu the super-large Sn-Cu polymetallic ore district. The main ore-hosting rocks are the carbonate rocks of the Middle Triassic Gejiu Formation and are characterized by the enrichment of Sn, Cu, Pb, Zn, Au and Ag (Zhao et al. 2022).

General appearance, crystal morphology, physical properties, and optical data

Cuprozheshengite occurs mainly as radial hemisphere aggregates with blade-like crystals. The hemispheres are typically 0.3 to 1 mm in diameter, and the individual blades have lengths up to 0.1–0.2 mm but widths of only 10 to 50 μm (Fig. 3). The triclinic crystals are flattened on (011) and elongated along [100].

Cuprozheshengite is transparent with a vitreous luster. The color is apple green to greenish blue, with a white streak. This mineral is brittle, with Mohs hardness 2½–3 and average Vickers hardness (VHN_{10g}) 129.2 ranging from 122.7–136.2 (in kg/mm^2, load in 10 g). Cuprozheshengite has {011} perfect cleavage and irregular fracture. The calculated density is 5.91 g/cm^3.

The indices of refraction could not be measured because they are greater than 1.80 and crystals of cuprozheshengite react in RI liquids greater than 1.80. The average index of refraction calculated using the Gladstone-Dale relationship Mandarino (1981) is 1.88. The $2V$ determined from extinction data using EXCALIBRW (Gunter et al. 2004) is 90.0(5)°.

MATERIALS AND ANALYTICAL METHODS

Materials

DC samples are deposited in the mineralogical collections of the Geological Museum of China, Yangrou hutong no. 15, Xisi, Xicheng District, Beijing, People's Republic of China, catalog no. M16127 (holotype) and the Crystal Structure Laboratory, China University of Geosciences, Beijing 100083, People's Republic of China, catalog no. DC4 (cotype); LC samples are deposited in the Natural History Museum of Los Angeles County, 900 Exposition Boulevard, Los Angeles, CA 90007, USA, catalog numbers 76191 and 76192 (cotype). The general appearance, crystal morphology, physical properties, and optical data, chemical composition and, crystal structure data of the LC sample are basically the same as those from the DC sample.

Chemical composition analysis

Backscattered electron (BSE) images and energy dispersive spectroscopy (EDS) line scanning of DC samples were obtained using a scanning electron microscope (SEM) (Mira XMU, TESCAN) at the School of Earth Sciences and Resources, China University of Geosciences.

The quantitative chemical composition data of the DC sample were determined at the electron probe micro-analysis laboratory, the China University of Geosciences, by an EPMA-1720 electron microprobe equipped with a wavelength dispersive spectrometer (WDS) at 15 kV, an electron beam current of 10 nA, and a beam diameter of 5 μm. The standards used are given in Table 1.

Raman spectrum analysis

The Raman spectrum of cuprozheshengite was obtained by HORIBA LabRAM HR Evolution Raman spectrometer in Via-Reflex, reflection mode with a laser excitation wavelength of 532 nm and 600 gr/mm. Spectrum in the 4000–200 cm^{-1} region was obtained by the collection time of 20 s and 2 scans with a resolution of 4 cm^{-1}.

Crystal structure analysis

A Rigaku XtaLAB PRO-007HF diffractometer was used for powder diffraction measurements using the rotating crystal method. The X-ray source was a rotating anode microfocus Mo*K*α at 50 kV and 24 mA, and the sensor was a hybrid pixel array detector. Cell parameters of powder diffraction data were refined by Chekcell software (Laugier and Bochu 2000). The calculated pattern was performed by the Powder cell software (Kraus and Nolze 1996).

The single-crystal X-ray analysis of the DC sample was done on the same diffractometer. Exposure time was 100 s per frame. An excellent quality 0.005 × 0.010 × 0.020 mm single-crystal fragment (This fragment was obtained from the zone close to the grain edge, where chemical composition data were determined and used to calculate the empirical formula. The crystal data mentioned in the main text were for this crystal and correspond to No. 11 in Table 8.) was selected to collect a full hemisphere of data ($-6 < h < 6$, $-11 < k < 10$, $-13 < l < 11$) with $R_{int} = 0.0520$. The intensity data were subjected to Lorentz-polarization and multi-scan absorption corrections. The crystal structure determination and refinement were performed using OLEX2-1.3 (Dolomanov et al. 2010) with SHELXT (Sheldrick 2015). The crystal

structure was solved using the intrinsic phasing method. The structure was refined to R = 0.039 based on 1588 independent reflections with $I > 2\sigma(I)$. The structure refinements confirmed the centrosymmetric space group P-1(#2). The crystal structure data of the DC sample is available in Online Materials CIF file.

Density functional theory (DFT) calculation

This work was done using the CASTEP code (Clark et al. 2005), and a plane wave basis was set up within the DFT scheme (Kohn and Sham 1965a, 1965b). Convergence testing showed a plane-wave basis represented by a kinetic energy cut-off of 400 eV; Total energy convergence tolerance is 10^{-6} eV; Eigen energy convergence tolerance is 2.205×10^{-7} eV. DFT calculations were performed to optimize the structure using energy minimization. We used the generalized gradient approximation (GGA) density functional, specifically Perdew, Burke, and Ernzerhof (PBE) (Perdew et al. 1996). The geometric optimization is performed by Broyden-Fletcher-Goldfarb-Shanno (BFGS). The details of BFGS are energy change per ion: dE/ion 10^{-5} eV; maximum force: $|F|_{max}$ 0.03 eV/Å; change in the distance: |dR| 0.001 Å. Spin-polarized parameters were considered. The modeling does not consider the H atom because it cannot be located at the appropriate position using energy minimization.

RESULTS AND DISCUSSION

Chemical composition

The BSE image (Fig. 4a) of the polished slice of the DC sample shows

concentric composition zones. EDS line scanning confirms that the nonuniform composition is mainly caused by variables P and As, and these two elements show a strong negative correlation (Fig. 4b). Twenty-five EPMA quantitative chemical data are obtained for the whole particle (marked in Fig. 4a) and the results of P and As content are shown in Figure 5. Most of the data are located in the cuprozheshengite region where the ratio of As: P ranges from 1: 3 to 3: 1; Two data are distributed in the left lower corner and identified as cuprodongchuanite; Another two data are scattered at the upper right corner, which could be an unnamed mineral with both *X* sites dominated by As. Limited by sample size, this unnamed mineral has not been confirmed by structure.

Considering the non-uniform composition of the sample, we selected ten analytic points to calculate the empirical formula (marked in the red circle in Fig.4) from one zone close to the grain edge where the single crystal XRD studied sample was performed with. The analytical results are given in Table 1. On the basis of O_{apfu} = 18, the empirical formula for the DC sample is $(Pb_{3.97}Na_{0.04}Ca_{0.01})_{\sum 4.02}Cu_{1.06}Zn_{2.09}(AsO_4)_2[(P_{0.84}As_{0.12}Si_{0.01})_{\sum 0.97}O_4]_2(OH)_2$. The simplified formula is $Pb_4CuZn_2[(As,P)O_4]_2[(P,As)O_4]_2(OH)_2$, and the ideal formula is $Pb_4CuZn_2(AsO_4)_2(PO_4)_2(OH)_2$, which requires PbO 58.55, ZnO 10.67, CuO 5.22, P_2O_5 9.31, As_2O_5 15.07, H_2O 1.18, total 100 wt.%.

H_2O was not determined directly. The Raman spectra of cuprozheshengite indicate the existence of only one kind of OH^-. Based on crystal-structure refinement and bond-valence sum (BVS), O9 is the only oxygen in the form of OH^-. Then we

calculate the total H_2O amount when the O9 site is fully occupied by OH^-.

The suggested Dana classification is 42.9 (Hydrated phosphates, etc., containing hydroxyl or halogen: $(AB)_7(XO_4)_4Z_q \cdot xH_2O$).

Raman spectroscopy

The Raman spectrum of cuprozheshengite is shown in Figure 6. The bands in the range from 600 to 450 cm^{-1} are assigned to the v_4 (and v_2) vibrations of the PO_4 (AsO_4) tetrahedrons, including 565, 541, 485, and 439 cm^{-1} (Frost et al. 2002; Ciesielczuk et al. 2016; Ismagilova et al. 2022); The band at 439 cm^{-1} probably corresponds to the symmetric stretching mode of the ZnO_4 tetrahedron (Hawthorne et al. 2012). Bands below 400 cm^{-1} at 386, 333 and 236 cm^{-1} can be assigned to lattice vibrations.

Bands in the range of 1100–600 cm^{-1} are ascribed to the mode vibrations of $(PO_4)^{3-}$ and $(AsO_4)^{3-}$ (Farmer 1974). Two groups of splitting peaks related to $(PO_4)^{3-}$ are confirmed to be v_3 (1062 and 1013 cm^{-1}) and v_1 (986, 967 and 947 cm^{-1}) mode, respectively. The peak at 833 cm^{-1} is assigned to the v_3 mode of $(AsO_4)^{3-}$ with a small shoulder at 795 cm^{-1}.

The only one sharp band at 3423 cm^{-1} is seen in the O–H stretching region, consistent with a single OH^- in the structure. The characteristic bending-mode vibration for H_2O at ~1600 cm^{-1} is absent (Grey et al. 2017).

Diffraction data and crystal structure

The observed and calculated X-ray powder diffraction data are provided in Table 2. The strongest eight X-ray powder-diffraction lines are bold. The refined unit-cell parameters from the powder-diffraction data are a = 4.7971(2), b = 8.5774(3), c = 10.3843(3) Å, α = 97.250(1)°, β = 101.890(1)°, γ = 91.500(1)°, and V = 414.1(5) $Å^3$.

The unit-cell parameters obtained for the DC sample from single-crystal XRD data are: a = 4.7977(8), b = 8.5789(8), c = 10.3855(9) Å, α = 97.270(8)°, β = 101.902(12)°, γ = 91.495(11)°, and V = 414.30(9) Å^3. The crystal structure description of the DC sample is reported here for the model in space group P-1(#2). Detailed information of the data collection and refinement are given in Table 3. The refined coordinates, refined occupancy and equivalent isotropic displacement parameters are listed in Table 4 and the anisotropic displacement parameters are listed in Table 5. Selected interatomic distances are reported in Table 6. Bond valence sums are reported in Table 7.

Dongchuanite group minerals form an isomorphous series, and cuprozheshengite is no exception. A projection of the structure along [100] is given in Figure 7. The structural framework is composed of two types of heteropolyhedral columns along [100], shown in Figure 7. The two types of columns are connected by corner-sharing between [$^{IV}BO_4$] and [$X1O_4$] tetrahedra to form layers parallel to (011). Type 1 columns are composed of corner-linked [$^{IV}BO_4$] and [$X2O_4$] tetrahedra. Each tetrahedron is 3-connected with other tetrahedra in the columns. Type 2 columns have alternating [$^{VI}BO_4(OH)_2$] octahedra with pairs of corner-connected [$X1O_4$] tetrahedra. The same type of column is present in many of the gadolinite supergroup minerals; for example, in drugmanite, [(Fe,Al)O_6] octahedra share corners with [PO_4] tetrahedra (King and Sengier-Roberts 1988). Pb atoms occupy two independent sites between the layers.

For the studied DC sample, chemical composition and structure refinement show

Cu and Zn fully occupy the ^{VI}B and ^{IV}B sites, respectively. The interatomic distances for the ^{VI}B site show four of ~2.0 Å and two much longer than 2.4 Å, characteristic of Jahn-Teller-distorted Cu^{2+} (Danisi et al. 2013). Site occupancy refinements and bond-valence sums indicate that one of the two independent *X* sites (*X*1) contains predominantly As. In contrast, the other *X* site (*X*2) is predominantly occupied by P. In the structure refinements, P and As were included at the two sites, and their occupancies were refined. The refined occupancy of *X*1 site is 0.764(11) As + 0.236(19) P and *X*2 site is 0.620(19) P + 0.382(11) As. Both Pb sites have lopsided coordinations typical of Pb^{2+} with stereo active $6s^2$ lone-pair electrons. Pb1 has four bonds to anions in the range 2.32 to 2.59 Å and three longer bonds in the range 2.94 to 3.09 Å, while Pb2 has four bonds in the range 2.35 to 2.55 Å and two longer bonds at 2.88 and 3.03 Å (Fig. 8). Similar bonding has been reported for Pb in drugmanite (King and Sengier-Roberts 1988). Raman spectrum (Fig. 6) and BVS (Table 7) confirm that H is attached to O9 as OH^-.

The geometric parameters of *X* sites and relationship with As and P

Two independent *X* sites (*X*1 and *X*2) are 4-coordinated and can be occupied by P and As. The ratio of P and As at each site can be studied by single-crystal XRD and quantified by structure refinement. Meanwhile, geometric parameters can also be obtained. Arsenic atoms tend to occupy the *X*1 site preferentially. This is not an isolated case, but a general phenomenon for dongchuanite group minerals. The results of single-crystal refinements of thirteen dongchuanite group mineral samples show that: If *apfu* of As is less than 0.8, it seems that no As atom is observed at the *X*2 site,

and nearly all As atoms occupy the *X*1 site. If *apfu* of As is beyond 1.0, a small amount of As occupies the *X*2 site, but the total As at the *X*2 site is always less than *X*1. The thirteen crystal structure results are presented in Table 8 and Figure 9, and the data show a linear correlation between the occupancy of As and the average bond length at each site (with an excellence-of-fit, R^2, 0.966 for *X*1 and 0.931 for *X*2 site, and the color bands are 90%, confidence bands). The fitting formulas are $y = 0.179\ x + 1.516$ (*X*1 site) and $y = 0.146\ x + 1.544$ (*X*2 site) (Fig. 10). When the occupancy of As is relatively low, the average bond length of the *X*1 site is shorter than that of the *X*2 site. In general, when the central ions are the same, the shorter the bond, the higher the bond energy, and the more energy it takes to break the bond, which means the more stable the substance is. In this case, arsenic atoms preferentially occupy the *X*1 site, which will undoubtedly get a more stable structure. But with the increasing occupancy of As, the slope of the *X*1 site fitting formula is steeper, and the average bond-length gap between the two sites is narrower. At this stage, the preference of As to occupy site *X*1 weakens, and As begins to occupy the *X*2 site.

DFT calculation

Our single-crystal XRD results suggest that when the As content is relatively low, As preferentially occupying the *X*1 site will contribute to structural stability. Therefore, we constructed three super-cell ($a = 2*a_0$, $c = 2*c_0$) models to compare the energy difference of As doping at *X*1 and *X*2 sites (Fig. 11). There are sixteen *X* sites in a supercell, among which *X*1 and *X*2 sites are 50% each. In the initial model (Model 0), the sixteen *X* sites are fully occupied by P. In Model 1, one *X*1 site is

replaced by As. In Model 2, one *X*2 site is replaced by As. After modeling, the energy minimization is performed to optimize the structure using DFT calculations, as shown in Table 9. The DFT-calculated geometric parameters are displayed in Table 10. Compared with the initial model, both Model 1 and Model 2 increase the system's energy. E_1 is 0.05 eV lower than E_2, which indicates that As atoms occupancy *X*1 site is thermodynamically favorable. This energy difference is relatively small, but only one-sixteenth As substitution is considered. Most natural minerals are stable, even if they are disordered when formed, but can diffuse to form thermally stable structures over time (Xian et al. 2022). DFT calculation reveals that As preferentially occupying the *X*1 site involves a thermodynamically favorable self-purification process. The DFT calculated average bond length is close to the linear fit predicted value, indicating the above linear fit is credible. Moreover, the cell volume of Model 1 is smaller than Model 2, implying that Model 1 is more stable.

Relationship to other mineral species

Structurally, cuprozheshengite is related to gadolinite supergroup minerals with similar type of heteropolyhedral columns (type 2) (Bacik et al. 2017). These minerals conform to the general formula $A_2MQ_2X_2O_8\varphi_2$, where A = Ca, REE, Pb, Bi; M = Fe, Mg, Zn, Cu, Al; Q = B, Be, Li; X = Si, P, As, B, Be and φ = O, OH, F. The minerals generally have monoclinic symmetry, $P2_1/c$, but triclinic examples have also been reported (Cooper et al. 2019). The unit-cell parameters of the gadolinite supergroup minerals are a = 4.6 to 4.8, b = 7.5 to 8.0, and c = 9.6 to 11.1 Å. Cuprozheshengite differs significantly from all gadolinite supergroup members in ordering different

atoms (P and As) in the two independent *X* sites in *P*-1.

Three other cuprozheshengite isomorphous minerals have been approved by IMA-CNMNC; dongchuanite, cuprodongchuanite, and zheshengite. There are enough members to establish a group. The general crystal chemistry formula of dongchuanite group minerals should be $A_4^{VI}B^{IV}B_2(X1O_4)_2(X2O_4)_2(OH)_2$ (Table 11). The EPMA data have confirmed that the exceptionally As-rich zone can make both *X*1 and *X*2 sites As dominant. However, structural evidence needs to be included. The minerals of the isomorphous series can be distinguished from each other using the As: P ratio determined from quantitative chemical analyses with P: As > 3:1 identified as the dongchaunite (cuprodongchuanite), those with P: As < 1:3 identified as the unnamed As-rich phase, and others between these two ranges qualified as zheshengite (cuprozheshengite) (Fig. 5).

IMPLICATIONS

Cuprozheshengite is a typical example of As-P ordering separation into different structural positions. It is classified based on the statistical rule of As occupying the *X*1 site preferentially. But we cannot prove that the As and P in dongchuanite group minerals are always ordered based on the structural data of a small number of samples. Strictly speaking, meaningful distributions of traits must be obtained from many individual specimens to distinguish distinct natural kinds. However, their type localities are often unitary for recently found new minerals, so there is no possibility of a sufficient amount of data for extensive study. The good sign is that the structural

geometric parameters and DFT calculation study of cuprozheshengite prove that the occupancy propensity of As is not an accidental phenomenon but a result of maintaining structural stability. So this study provides a new idea for studying other rare minerals with P-As atoms ordering at different sites based on limited data.

Based on the crystal structure study of natural minerals, effective methods will be found for disposing of high-level waste pollution, mainly by immobilizing them within natural crystalline matrixes (Khomyakov 2008). The preferential occupation of the *X*1 position by As in cuprozheshengite may indicate a more efficient structural unit (type 2 column) to accommodate As. The type 2 column is also present in many gadolinite supergroup minerals (Bacik et al. 2017), suggesting their utility for As fixation. Meanwhile, the cuprozheshengite has a unique combination of elements. In addition to As, it contains heavy metals like Pb, Zn, and Cu, and can be a candidate material for comprehensive environmental governance. It is the only known inorganic crystal (ICSD and Mindat database) with independent crystallographic sites of Pb, Zn, Cu, As and P. As a stable mineral in the water and elemental cycles after weathering, cuprozheshengite still has the potential to continually crystallize in the local area. By converting waste pollution into a crystalline form, humans can maintain favorable environmental conditions comparable to geological periods on Earth.

ACKNOWLEDGMENTS

We are grateful to Prof. Ritsuro Miyawaki and his colleagues for their valuable suggestions regarding cuprozheshengite. Additionally, we would like to thank Xiang

Wu and Zhaochu Hu for their help with the Raman analysis of cuprozheshengite. The National Natural Science Foundation of China (41672043) supported this research.

REFERENCES CITED

Allmann, R. (1975) Beziehungen zwischen Bindungslängen und Bindungsstärken in Oxidstrukturen. Monatshefte für Chemie, 106, 779–793.

Antelo, J., Arce, F., and Fiol, S. (2015) Arsenate and phosphate adsorption on ferrihydrite nanoparticles. Synergetic interaction with calcium ions. Chemical Geology, 410, 53–62.

Bacik, P., Miyawaki, R., Atencio, D., Camara, F. and Fridrichova, J. (2017) Nomenclature of the gadolinite supergroup. European Journal of Mineralogy, 29, 1–16.

Bajda, T., Mozgawa, W., Manecki, M., and Topolska, J. (2011) Vibrational spectroscopic study of mimetite–pyromorphite solid solutions. Polyhedron, 30, 2479–2485.

Biagioni, C., Bosi, F., Hålenius, U., and Pasero, M. (2016) The crystal structure of svabite, $Ca_5(AsO_4)_3F$, an arsenate member of the apatite supergroup. American Mineralogist, 101, 1750–1755.

Brown, I.D. (1977) Predicting bond lengths in inorganic crystals. Acta Crystallographica Section B-Structural Science Crystal Engineering and Materials, 33, 1305–1310.

Brown, I.D. and Altermatt, D. (1985) Bond-valence parameters obtained from a

systematic analysis of the inorganic crystal structure database. Acta Crystallographica Section B-Structural Science Crystal Engineering and Materials, 41, 244–247.

Ciesielczuk, J., Janeczek, J., Dulski, M., and Krzykawski, T. (2016) Pseudomalachite–cornwallite and kipushite–philipsburgite solid solutions: chemical composition and Raman spectroscopy. European Journal of Mineralogy, 28, 555–569.

Clark, S.J., Segall, M.D., Pickard, C.J., Hasnip, P.J., Probert, M.J., Refson, K., and Payne, M.C. (2005) Castep v5.0. Zeitschrift für Kristallographie, 220, 567–570.

Cooper, M.A., Hawthorne, F.C., Miyawaki, R. and Kristiansen, R. (2019) Cation order in the crystal structure of "Ca-hingganite-(Y)". The Canadian Mineralogist, 57, 371–382.

Danisi, R.M., Armbruster, T., Lazic, B., Vulic, P., Kaindl, R., Dimitrijevic, R. and Volker, K. (2013) In situ dehydration behavior of veszelyite $(Cu,Zn)_2Zn(PO_4)(OH)_3 \cdot 2H_2O$: a single-crystal X-ray study. American Mineralogist, 98, 1261–1269.

Dolomanov, O.V., Bourhis, L.J., Gildea, R.J., Howard, J., and Puschmann, H. (2010) Olex2: a complete structure solution, refinement and analysis program. Journal of Applied Crystallography, 42, 339–341.

Farmer, C.V. (1974) The Infrared Spectra of Minerals. Mineralogical Society of Minerals Monograph 4, The Mineralogical Society, London, 539 p.

Frost, R.L., Martens, W.N., and Williams, P.A. (2002) Raman spectroscopy of the phase-related basic copper arsenate minerals olivenite, cornwallite, cornubite and

clinoclase. Journal of Raman Spectroscopy, 33, 475–484.

Grey, I.E., Keck, E., Kampf, A.R., Macrae, C.M., Glenn, A.M., and Price, J.R. (2017). Wilhelmgümbelite, $[ZnFe^{2+}Fe_3^{3+}(PO_4)_3(OH)_4(H_2O)_5]\cdot 2H_2O$, a new schoonerite-related mineral from the Hagendorf süd pegmatite, Bavaria. Mineralogical Magazine, 81, 287–296.

Gunter, M.E., Bandli, B.R., Bloss, F.D., Evans, S.H., Su, S.C. and Weaver, R. (2004) Results from a McCrone spindle stage short course, a new version of EXCALIBR, and how to build a spindle stage. The Microscope, 52, 23−39.

Hawthorne, F.C., Cooper, M.A., Abdu, Y.A., Ball, N.A., Back, M.E., and Tait, K.T. (2012) Davidlloydite, ideally $Zn_3(AsO_4)_2(H_2O)_4$, a new arsenate mineral from the Tsumeb mine, Otjikoto (Oshikoto) region, Namibia: description and crystal structure. Mineralogical Magazine, 76, 45–57.

Hitzman, M.W., Kirkham, R., Broughton, D., Thorson, J., and Selley, D. (2005) The sediment-hosted stratiform copper ore system: Economic Geology 100th Anniversary Volume, 609−642.

Ismagilova, R., Rieck, B., Kampf, A., Giester, G., Zhitova, E., Lengauer, C., Krivovichev, S.V., Zolotarev, A.A., Ciesielczuk, J., Mikhailova, J.A., Bocharov, V.N., Shilovskikh, V.V., Vlasenko, N.S., Nash, B.P., and Adams, P. (2022) Goldhillite, $Cu_5Zn(AsO_4)_2(OH)_6\cdot H_2O$, a new mineral species, and redefinition of philipsburgite, $Cu_5Zn[(AsO_4)(PO_4)](OH)_6\cdot H_2O$, as an As–P ordered species. Mineralogical Magazine, 86, 436−446.

Khomyakov, A. (2008) The Largest Source of Minerals with Unique Structure and

Properties. Minerals as Advanced Materials. Doi: 10.1007/978-3-540-77123-4_9.

King, G.S.D. and Sengier-Roberts, L. (1988) Drugmanite, $Pb_2(Fe_{0.78}Al_{0.22})H(PO_4)_2(OH)_2$: Its crystal structure and place in the datolite group. Bulletin de Mineralogie, 111, 431−437.

Kocourkova-Vikova, E., Loun, J., Sracek, O., Houzar, S., and Filip, J. (2015) Secondary arsenic minerals and arsenic mobility in a historical waste rock pile at Kank near Kutna Hora, Czech Republic. Mineralogy and Petrology, 109, 17–33.

Kohn, W. and Sham, L.J. (1965a) Self-consistent equations including exchange and correlation effects. Physical Review, 140(4A), A1133–A1138.

Kohn, W. and Sham, L.J. (1965b) Quantum density oscillations in an inhomogeneous electron gas. Physical Review, 137(6A), A1697–A1705.

Kraus, W. and Nolze, G. (1996) POWDER CELL–a program for the representation and manipulation of crystal structures and calculation of the resulting X-ray powder patterns. Journal of Applied Crystallography, 29, 301–303.

Krivovichev, S.V. (2012) Derivation of bond-valence parameters for some cation-oxygen pairs on the basis of empirical relationships between r_o and b. Zeitschrift für Kristallographie - Crystalline Materials, 227, 575–579.

Krivovichev, S.V. and Brown, I.D. (2001) Are the compressive effects of encapsulation an artifact of the bond valence parameters? Zeitschrift Fur Kristallographie, 216, 245–247.

Krivovichev, S.V., Zhitova, E.S., Ismagilova, R.M., and Zolotarev, A.A. (2018) Site-selective As–P substitution and hydrogen bonding in the crystal structure of

philipsburgite, $Cu_5Zn((As,P)O_4)_2(OH)_6 \cdot H_2O$. Physics and Chemistry of Minerals, 45, 917–923.

Kunhikrishnan, A., Choppala, G., Seshadri, B., Wijesekara, H., Bolan, N.S., Mbene, K., and Kim, W.-I. (2017) Impact of wastewater derived dissolved organic carbon on reduction, mobility, and bioavailability of As(V) and Cr(VI) in contaminated soils. Journal of Environmental Management, 186(2), 183–191.

Laugier, J., and Bochu, B. (2000) CHECKCELL – A Software Performing Automatic Cell/Space Group Determination, Collaborative Computational Project Number 14 (CCP14), Laboratoiredes Matériaux et du Génie Physique de l'Ecole Superieure de Physique de Grenoble (INPG), France.

Legrand, P. (2017) XDSME: XDS Made Easier, GitHub repository, https://github.com/legrandp/xdsme. Doi: 10.5281/zenodo.837885.

Li, G., Sun, N., Shen, H., Xue, Y. and Hao, J. (2022) Zheshengite, IMA 2022-011, in: CNMNC Newsletter 67. European Journal of Mineralogy, 34.

Ma, Z., Li, G., Chukanov, N.V., Poirier, G., and Shi, N. (2014) Tangdanite, a new mineral species from the Yunnan province, china and the discreditation of 'clinotyrolite'. Mineralogical Magazine, 78, 559–570.

Mandarino, J.A. (1981) The Gladstone-Dale relationship: Part IV. The compatibility concept and its application. The Canadian Mineralogist, 19, 441–450.

Perdew, J.P., Burke, K., and Ernzerhof, M. (1996) Generalized gradient approximation made simple. Physical Review Letters, 77, 3865–3868.

Rakovan, J.F., and Pasteris, G.D. (2015) A technological gem: Materials, medical, and environmental mineralogy of apatite. Elements, 11, 195–200.

Sheldrick, G.M. (2015) Crystal structure refinement with shelxl. Acta Crystallographica Section C-Structural Chemistry, 71, 3–8.

Siidra, O.I., Nazarchuk, E.V., Pautov, L.A., Borisov, A.S., and Kozin, M.S. (2021) Milkovoite, IMA 2021-005. CNMNC Newsletter 61. Mineralogical Magazine, 85, 299–304.

Xian, H., He, H., Qiu, K., Li, Y., Yang, Y., Xie, J., Tan, W., Tsuchiyama, A., Yastake, M., Enju, S., Miyake, A., and Zhu, R. (2022) Hyperenrichment of gold in pyrite induced by solid-state transportation. Communications Earth & Environment, 3, 308.

Xing, S., Guo, H., Zhang, L., Wang, Z., Sun, X. (2022) Silicate weathering contributed to arsenic enrichment in geotherm-affected groundwater in Pliocene aquifers of the Guide basin, China. Journal of Hydrology, 606.

Yakovenchuk, V.N., Pakhomovsky, Y.A., Konoplyova, N.G., Panikorovskii, T.L., Mikhailova, Y.A, Bocharov, V.N, Krivovichev, S.V and Ivanyuk, G.Y. (2017) Epifanovite $NaCaCu_5(PO_4)_4[AsO_2(OH)_2]\cdot 7H_2O$, a new mineral from the Kester deposit (Sakha-Yakutia, Russia). Zapiski Rossiiskogo Mineralogicheskogo Obshchetstva, 146, 30–39 [in Russian].

Liang, X., Lin, X., Wei, G., Ma, L., He, H., Carballal, D.S., Zhu, J., Zhu, R., and Leeuw, N.D. (2021) Competitive adsorption geometries for the arsenate As(V) and phosphate P(V) oxyanions on magnetite surfaces: Experiments and theory.

American Mineralogist, 106, 374–388.

Zhao, Y., Tian, H., Li, J., Chen, S., Zhao, J. (2022) Constraints on the genesis of the Laochang Pb–Zn ore, Gejiu district, Yunnan: Evidence from sulfide trace element and isotope geochemistry. Ore Geology Reviews, 150, 105162.

Zhao M., and Yang Y. (2022) Health Risk Assessment of Heavy Metals in the Main River Basins of Dongchuan, Yunnan Province. Chinese Journal of Inorganic Analytical Chemistry, 12, 26–33 [in Chinese].

Zhao, X., Zhou, M., Li, J., Sun, M., Gao, J., Sun, W., and Yang, J. (2010) Late Paleoproterozoic to early Mesoproterozoic Dongchuan Group in Yunnan, SW China: Implications for tectonic evolution of the Yangtze block: Precambrian Research, 182, 57–69.

Zhao, X., Zhou, M., Hitzman, M.W., Li, J., Bennett, M., Meighan, C., and Anderson, E. (2012) Late Paleoproterozoic to Early Mesoproterozoic Tangdan Sedimentary Rock-Hosted Strata-bound Copper Deposit, Yunnan Province, Southwest China. Economic Geology, 107, 357–375.

TABLE CAPTIONS

Table 1. Chemical data (in wt.%) for cuprozheshengite (DC).

Table 2. X-ray powder diffraction data (*d* in Å) for cuprozheshengite (DC).

Table 3. Crystal data and structure refinement for cuprozheshengite (DC).

Table 4. Atomic coordinates and site occupancies for cuprozheshengite (DC).

Table 5. Anisotropic displacement parameters (in $Å^2$) for cuprozheshengite (DC).

Table 6. Selected geometric parameters (Å) for cuprozheshengite (DC).

Table 7. Bond-valence sum for cuprozheshengite (DC).

Table 8. The occupancy of *X* site and average bond length of *X*–O of cuprozheshengite isomorphous minerals.

Table 9. Total energy differences (eV) after geometry optimization of the three models.

Table 10. The geometric parameters after geometry optimization of the three models.

Table 11. Members and potential members of cuprozheshengite isomorphous minerals ($A_4B^{VI}B^{IV}{}_2(X1O_4)_2(X2O_4)_2(OH)_2$).

FIGURE CAPTIONS

Figure 1. (a) A view of the dump. (b) The mine entrance. (c). A vein is rich in sulfide minerals. (d) Plentiful supergene minerals form in a sandstone fracture around Cu-sulphide ore veins.

Figure 2. (a) Apple-green spherical radial aggregates of cuprozheshengite (Czs) associated with hemimorphite (Hmp) and veszelyite (Vsz) from Dongchaun. (b) Greenish-blue hemispheres of cuprozheshengite (Czs) on white hemimorphite (Hmp) associated with dark blue crystals of veszelyite (Vsz) from Laochang.

Figure 3. Scanning electron microscope image of aggregate of cuprozheshengite blades from Laochang.

Figure 4. Backscattered electron (BSE) image and energy dispersive spectroscopy (EDS) line scanning of cuprozheshengite aggregate (polished slice). (a) Obvious

zones are shown on the BSE image. Twenty-five white points are EPMA tested areas. Ten red circles are the selected data for empirical formula calculation. (b) EDS line scanning confirms that the nonuniform of the composition is mainly caused by P and As. There is a strong negative correlation between these two elements. The distributions of Cu, Zn, Pb and O are almost uniform.

Figure 5. Scatter diagram of *apfu* P and As calculated from the twenty-five EPMA points respectively (Corresponding to the analysis points in Figure 4).

Figure 6. Raman spectrum of cuprozheshengite.

Figure 7. [100] projection of the crystal structure of cuprozheshengite with atom labelling and two types of 4.7 Å columns in cuprozheshengite structure.

Figure 8. Schematic representation of [PbO_n] polyhedra. O9 is water oxygen-atoms OH. Solid lines: short Pb–O bonds; dotted lines: long Pb–O bonds.

Figure 9. The distribution of As atoms at *X*1 and *X*2 sites based on thirteen X-ray crystal structure refinement of cuprozheshengite isomorphous mineral (data in Table 8). The results show that As atoms tend to occupy *X*1 position preferentially.

Figure 10. Linear correlation between the occupancy of As and the average bond length at each site and fitting formulas (the color bands are 90% confidence bands).

Figure 11. Three super-cell (a = 2*a_0, c = 2*c_0) models.

Table 1. Chemical data (in wt.%) for cuprozheshengite (DC).

Constituent	Mean	Range	Stand. Dev. (σ)	Reference Material
Na_2O	0.08	0.07−0.09	0.01	Albite
V_2O_5	0.01	0.00−0.06	0.02	Vanadium
SiO_2	0.10	0.03−0.17	0.04	Sanidine
CuO	5.46	5.20−5.68	0.13	Chalcopyrite
As_2O_5	16.52	14.82−20.47	1.71	Cobaltite
FeO	0.02	0.00−0.08	0.03	Garnet
P_2O_5	7.73	5.38−8.85	1.08	Apatite
ZnO	10.95	10.54−11.47	0.28	Willemite
SO_3	0.00	0.00−0.00	0.00	Barite
PbO	57.16	56.09−58.16	0.65	Crocoite
CaO	0.03	0.01−0.06	0.02	Apatite
BaO	0.01	0.00−0.03	0.01	Barite
H_2O*	1.16			
Total	99.24	98.77−99.74	0.34	

Note: The data in this table corresponded to ten red-circled analysis points in Figure 4.

Table 2. X-ray powder diffraction data (*d* in Å) for cuprozheshengite (DC).

I_{obs}	I_{calc}	d_{obs}	d_{calc}	*h*	*k*	*l*	I_{obs}	I_{calc}	d_{obs}	d_{calc}	*h*	*k*	*l*
5	1	8.7519	8.4966	0	-1	0	1	1	1.3500	1.3511	-1	6	1
7	2	6.9733	6.9723	0	-1	1	6	7	1.3283	1.3280	0	5	4
21	**8**	**6.1102**	**6.1016**	**0**	**1**	**1**	7	10	1.2905	1.2918	3	-2	3
9	2	5.0091	5.0345	0	0	2	4	4	1.2811	1.2806	-3	4	2
30	**26**	**4.6413**	**4.6409**	**-1**	**0**	**1**	1	4	1.2616	1.2616	-3	1	6
11	7	4.2427	4.2483	0	2	0	4	4	1.2432	1.2437	-1	6	3
19	13	4.0939	4.0963	0	1	2	3	10	1.2220	1.2221	-3	3	5
7	8	3.9230	3.9429	1	0	1	11	9	1.1871	1.1871	-4	0	3
7	4	3.7428	3.7382	0	2	1	8	11	1.1633	1.1632	-1	-7	3
100	**100**	**3.4413**	**3.4398**	**-1**	**1**	**2**	5	3	1.1365	1.1366	-1	5	6
34	**24**	**3.2669**	**3.2758**	**0**	**-1**	**3**	10	7	1.1073	1.1075	0	-7	5
89	**65**	**3.0544**	**3.0508**	**-1**	**0**	**3**	3	2	1.0802	1.0801	4	2	1
61	**59**	**2.9479**	**2.9450**	**-1**	**-2**	**2**	1	9	1.0707	1.0703	-4	3	4
44	**46**	**2.8173**	**2.8205**	**1**	**1**	**2**	4	1	1.0632	1.0628	-4	-3	0
14	14	2.6227	2.6238	0	-3	2	4	8	1.0499	1.0498	0	-4	9
12	11	2.5039	2.5072	0	-1	4	1	10	1.0437	1.0435	1	-2	9
15	44	2.3856	2.3820	-2	0	1	2	9	1.0283	1.0281	1	6	5
20	**27**	**2.3216**	**2.3210**	**0**	**1**	**4**	3	2	1.0078	1.0076	-1	1	10
6	12	2.2757	2.2806	1	-2	3	3	4	0.9936	0.9936	3	5	3
4	8	2.2189	2.2185	-1	-2	4	3	2	0.9842	0.9845	0	1	10
7	4	2.1646	2.1724	-1	-3	3	2	2	0.9772	0.9769	-1	8	3
1	3	2.0930	2.0991	-2	-1	3	1	1	0.9653	0.9654	2	2	8
8	10	2.0422	2.0441	-2	-2	2	7	7	0.9473	0.9474	0	6	7
12	23	2.0122	2.0106	-1	0	5	2	8	0.9331	0.9325	2	-5	8
6	13	1.9423	1.9445	-2	-2	3	4	6	0.9201	0.9197	-3	-3	10
12	18	1.9014	1.9010	-1	-2	5	1	2	0.9069	0.9067	-4	-6	3
6	22	1.8512	1.8508	-2	3	1	3	2	0.8954	0.8952	1	8	4
5	11	1.8104	1.8094	-2	-3	1	2	5	0.8841	0.8838	1	-8	7
15	14	1.7326	1.7330	-1	-3	5	2	6	0.8762	0.8761	-2	-9	3
8	9	1.6794	1.6800	0	-5	2	2	3	0.8697	0.8696	-3	3	10
15	18	1.6243	1.6258	1	-5	0	1	1	0.8641	0.8644	-5	-4	2
10	12	1.5712	1.5707	0	-4	5	4	1	0.8578	0.8580	-1	0	12
15	26	1.5103	1.5107	-3	2	1	5	1	0.8386	0.8386	0	3	11
8	3	1.4824	1.4826	-2	4	3	2	2	0.8324	0.8324	1	7	7
5	13	1.4656	1.4655	2	4	1	3	2	0.8264	0.8260	3	-3	9
3	9	1.4427	1.4415	-3	-2	0	4	3	0.8209	0.8209	-1	2	12
10	5	1.3955	1.3956	2	-5	1	4	2	0.7998	0.7997	-5	4	7
6	14	1.3697	1.3698	-1	-3	7							

Table 3. Crystal data and structure refinement for cuprozheshengite (DC).

Crystal data	
Chemical formula	$Pb_4CuZn_2[(As_{0.764(11)}P_{0.236(19)})O_4]_2[P_{0.620(19)}(As_{0.382(11)})O_4]_2(OH)_2$
Formula weight	1535.57
Crystal system, space group	Triclinic, *P*-1
Temperature (K)	293
a, *b*, *c* (Å)	4.7977 (8), 8.5789 (8), 10.3855 (9)
α, *β*, *γ* (°)	97.270 (8), 101.902 (12), 91.495 (11)
V (Å^3)	414.30 (9)
Z	1
Radiation type	Mo*K*α
m (mm^{-1})	49.39
Crystal size (mm)	0.020 × 0.010 × 0.005
Data collection	
Diffractometer	XtaLAB PRO-007HF
Absorption correction	Multi-scan
T_{min}, T_{max}	0.720, 1.000
No. of measured, independent and observed [$I > 2\sigma(I)$] reflections	3983, 1885, 1588
R_{int}	0.052
$(\sin \theta/\lambda)_{max}$ (Å^{-1})	0.682
Refinement	
$R[F^2 > 2\sigma(F^2)]$, $wR(F^2)$, S	0.039, 0.088, 1.07
No. of reflections	1885
No. of parameters	137
No. of restraints	2
$\Delta\rho_{max}$, $\Delta\rho_{min}$ (e Å^{-3})	2.51, –1.82

Table 4. Atomic coordinates and site occupancies for cuprozheshengite (DC).

Site	Atom	*Wyck.*	*Occ.*	*x/a*	*y/b*	*z/c*	U_{eq}
A	Pb1	2*i*	1	-0.14793(10)	0.51824(5)	0.17173(4)	0.02126(14)
	Pb2	2*i*	1	-0.11198(10)	0.10414(6)	0.33840(5)	0.02464(15)
^{VI}B	Cu	1*c*	1	0	0.5	0.5	0.0178(4)
^{IV}B	Zn	2*i*	1	0.6705(3)	0.13034(16)	0.88246(14)	0.0208(3)
*X*1	As1	2*i*	0.764(11)	0.4869(3)	0.24782(16)	0.58750(13)	0.0160(5)
	P1	2*i*	0.236(19)	0.4869(3)	0.24782(16)	0.58750(13)	0.0160(5)
*X*2	P2	2*i*	0.620(19)	0.2443(4)	0.2205(2)	1.06586(19)	0.0184(7)
	As2	2*i*	0.382(11)	0.2443(4)	0.2205(2)	1.06586(19)	0.0184(7)
	O1	2*i*	1	0.3303(18)	0.0959(10)	1.1672(10)	0.028(2)
	O2	2*i*	1	-0.0927(17)	0.2433(10)	1.0452(9)	0.024(2)
	O3	2*i*	1	0.3900(16)	0.3891(10)	1.1249(9)	0.026(2)
	O4	2*i*	1	0.2959(17)	0.1602(11)	0.9220(8)	0.028(2)
	O5	2*i*	1	0.708(2)	0.2205(11)	0.7241(9)	0.031(2)
	O6	2*i*	1	0.6624(18)	0.2798(10)	0.4747(8)	0.0227(18)
	O7	2*i*	1	0.2460(16)	0.0987(10)	0.5298(9)	0.0235(19)
	O8	2*i*	1	0.3095(17)	0.4054(9)	0.6254(8)	0.0199(17)
	O9(OH)	2*i*	1	0.0829(16)	0.3848(9)	0.3407(8)	0.0173(17)

Table 5. Anisotropic displacement parameters (in Å^2) for cuprozheshengite (DC).

Site	Atom	U^{11}	U^{22}	U^{33}	U^{23}	U^{13}	U^{12}
A	Pb1	0.0245(3)	0.0210(3)	0.0175(2)	0.00500(19)	0.00132(18)	0.00095(18)
	Pb2	0.0254(3)	0.0228(3)	0.0233(3)	0.0021(2)	0.0004(2)	-0.00146(19)
^{VI}B	Cu	0.0197(10)	0.0191(11)	0.0126(9)	-0.0002(8)	0.0002(8)	0.0028(8)
^{IV}B	Zn	0.0229(7)	0.0211(8)	0.0167(7)	0.0024(6)	0.0008(5)	0.0002(6)
*X*1	As1	0.0169(7)	0.0166(8)	0.0137(7)	0.0040(5)	0.0005(5)	0.0010(5)
	P1	0.0169(7)	0.0166(8)	0.0137(7)	0.0040(5)	0.0005(5)	0.0010(5)
*X*2	P2	0.0184(11)	0.0188(12)	0.0165(11)	0.0020(8)	0.0006(7)	0.0016(7)
	As2	0.0184(11)	0.0188(12)	0.0165(11)	0.0020(8)	0.0006(7)	0.0016(7)
	O1	0.023(5)	0.022(5)	0.039(5)	0.008(4)	0.003(4)	0.001(4)
	O2	0.020(4)	0.021(5)	0.029(5)	-0.004(4)	0.004(4)	-0.002(3)
	O3	0.022(5)	0.021(5)	0.030(5)	-0.008(4)	0.002(4)	-0.008(4)
	O4	0.022(5)	0.043(6)	0.016(4)	-0.003(4)	0.003(4)	0.006(4)
	O5	0.039(5)	0.039(6)	0.015(4)	0.004(4)	0.006(4)	0.005(4)
	O6	0.033(5)	0.022(5)	0.016(4)	0.006(4)	0.010(4)	0.008(4)
	O7	0.015(4)	0.025(5)	0.031(5)	0.008(4)	0.003(4)	0.003(3)
	O8	0.028(5)	0.014(4)	0.018(4)	0.001(3)	0.006(3)	0.010(3)
	O9(OH)	0.023(4)	0.010(4)	0.017(4)	0.000(3)	0.002(3)	0.001(3)

Table 6. Selected geometric parameters (Å) for cuprozheshengite (DC).

Pb1—O2^{i}	2.599 (8)	Pb2—O1^{ii}	2.885 (9)
Pb1—O3^{ii}	2.381 (7)	Pb2—O1^{i}	3.034 (9)
Pb1—O3^{i}	2.942 (8)	Pb2—O6^{v}	2.494 (8)
Pb1—O4^{iii}	3.091 (10)	Pb2—O6	2.350 (9)
Pb1—O5^{iv}	2.974 (10)	Pb2—O7^{vi}	2.371 (8)
Pb1—O8^{iii}	2.413 (8)	Pb2—O9	2.555 (8)
Pb1—O9	2.322 (8)	**<Pb2–O>**	**2.615**
<Pb1–O>	**2.675**		
Cu—O7^{iv}	2.409 (9)	Zn—O1^{vii}	1.944 (9)
Cu—O7^{vi}	2.409 (9)	Zn—O2^{viii}	1.955 (9)
Cu—O8	2.023 (8)	Zn—O4	1.940 (8)
Cu—O8^{iii}	2.023 (8)	Zn—O5	1.942 (9)
Cu—O9	1.936 (8)	**<Zn–O>**	**1.945**
Cu—O9^{iii}	1.936 (8)		
<Cu–O>	**2.123**		
As1|P1–O5	1.634 (9)	P2|As2–O1	1.597 (9)
As1|P1–O6	1.665 (8)	P2|As2–O2	1.607 (8)
As1|P1–O7	1.623 (8)	P2|As2–O3	1.582 (8)
As1|P1–O8	1.664 (8)	P2|As2–O4	1.589 (9)
<As1|P1–O>	**1.647**	**<P2|As2–O>**	**1.594**

Symmetry codes: (i) x, y, z-1; (ii) x-1, y, z-1; (iii) -x, -y+1, -z+1; (iv) -x+1, -y+1, -z+1; (v) -x, -y, -z+1; (vi) x-1, y, z; (vii) -x+1, -y, -z+2; (viii) x+1, y, z; (ix) x+1, y, z+1; (x) x, y, z+1; (xi) -x+1, -y, -z+1.

Table 7. Bond-valence sum for cuprozheshengite (DC).

	Pb1	Pb2	Cu(^{VI}B)	Zn(^{IV}B)	As1|P1(X1)	P2|As2(X2)	**O sum**
O1		0.153+0.113		0.503		1.251	**2.020**
O2	0.274			0.488		1.217	**1.978**
O3	0.426+0.136					1.296	**1.858**
O4	0.100			0.507		1.277	**1.883**
O5	0.127			0.504	1.366		**1.960**
O6		0.454+0.338			1.335		**2.012**
O7		0.435	0.131×2↓→		1.258		**2.065**
O8	0.400		0.388 ×2↓ ×1→		1.148		**2.011**
O9	0.582	0.299	0.496 ×2↓ ×1→				**1.276**
Sum	**1.944**	**1.791**	**2.030**	**2.002**	**5.138**	**5.042**	

Note: The occupancy of X1 site is 0.764(11) As + 0.236(19) P and X2 site is 0.764(11) P + 0.236(19). The bond-valence calculations were done using the equation and constants of Brown (1977), $S = \exp[R_0 - d_0)/b]$. Bond parameters: Pb^{2+}–O^{2-} from Krivovichev and Brown (2001); Cu^{2+}–O^{2-} Krivovichev (2012); Zn^{2+}–O^{2-} from Allmann (1975); P^{5+}–O^{2-} from Gagne and Hawthorne (2015) and As^{5+}–O^{2-} Brown and Altermatt (1985).

Table 8. The occupancy of *X* site and average bond length of *X*–O of cuprozheshengite isomorphous minerals.

No.	Species	Occupancy of *X*1 site	Average bond length of *X*1–O (Å)	Occupancy of *X*2 site	Average bond length of *X*2–O (Å)
1	Dongchuangite	0.64(2)P+0.364(19)As	1.584	1.00P	1.546
2	Cuprodongchuanite	0.85(2)P+0.15(2)As	1.547	1.00P	1.546
3	Cuprodongchuanite	0.86(2)P+0.142(17)As	1.548	1.00P	1.546
4	Cuprodongchuanite	0.63(3)P+0.37(2)As	1.569	1.00P	1.540
5	Zheshengite	0.31(2)P+0.686(12)As	1.642	0.86(2)P+0.144(12)As	1.570
6	Zheshengite	0.32(2)P+0.678(17)As	1.636	0.82(2)P+0.178(16)As	1.573
7	Zheshengite	0.29(2)P+0.713(17)As	1.657	0.81(2)P+0.187(16) As	1.570
8	Cuprozheshengite	0.29(2)P+0.705(19)As	1.642	0.66(2)P+0.340(19)As	1.584
9	Cuprozheshengite	0.40(2)P+0.604(16)As	1.616	0.78(2)P+0.224(16) As	1.575
10	Cuprozheshengite	0.19(2)P+0.810(18)As	1.673	0.55(2)P+0.451(18)As	1.624
11	Cuprozheshengite	0.236(19)P+0.764(11)As	1.647	0.620(19)P+0.382(11)As	1.594
12	Cuprozheshengite	0.28(2)P+0.719(15)As	1.644	0.80(2)P+0.197(15)As	1.566
13	Cuprozheshengite	0.36(2)P+0.64(2)As	1.625	0.91(1)P+0.09(1)As	1.558

Table 9. Total energy differences (eV) after geometry optimization of the three models.

E_1–E_0	E_2–E_0	E_1–E_2
11.51	11.56	-0.05

Table 10. The geometric parameters after geometry optimization of the three models.

	Model 0	Model 1	Model 2
a (Å)	9.8537	9.8747	9.8629
b (Å)	8.7356	8.7337	8.7584
c (Å)	21.1501	21.1623	21.1662
α (°)	96.9004	96.868	96.911
β (°)	105.1132	105.1499	105.0189
γ (°)	89.7405	89.801	89.7882
V(Å^3)	1744.1765	1748.2865	1752.3957
Average bond length of *X*1–O	1.539 (P–O)	1.703 (As–O)	1.539(P–O)
Expected bond length of *X*1–O*		1.516 (P–O) 1.695 (As–O)	
Average bond length of *X*2–O	1.541 (P–O)	1.541 (P–O)	1.704 (As–O)
Expected bond length of *X*2–O*		1.544 (P–O) 1.690 (As–O)	

*Calculated by fitting formulas

Table 11. Members and potential members of cuprozheshengite isomorphous minerals ($A_4B^{VI}B^{IV}{}_2(X1O_4)_2(X2O_4)_2(OH)_2$).

B^{VI}	***X*1 =*X*2 = P**	***X*1 = As, *X*2 = P**	***X*1 =*X*2 = As**
Zn	Dongchuanite (IMA2021-058) $Pb_4{}^{VI}Zn^{IV}Zn_2(PO_4)_2(PO_4)_2(OH)_2$	Zheshengite (IMA2022-011) $Pb_4{}^{VI}Zn^{IV}Zn_2(AsO_4)_2(PO_4)_2(OH)_2$	Full As analogue of dongchuanite (Potential) $Pb_4{}^{VI}Zn^{IV}Zn_2(AsO_4)_2(AsO_4)_2(OH)_2$
Cu	Cuprodongchuanite (IMA2021-065) $Pb_4{}^{VI}Cu^{IV}Zn_2(PO_4)_2(PO_4)_2(OH)_2$	Cuprozheshengite (IMA2022-095a) $Pb_4{}^{VI}Cu^{IV}Zn_2(AsO_4)_2(PO_4)_2(OH)_2$	Full As analogue of cuprodongchuanite (Potential) $Pb_4{}^{VI}Cu^{IV}Zn_2(AsO_4)_2(AsO_4)_2(OH)_2$

Figure 1

Figure 2

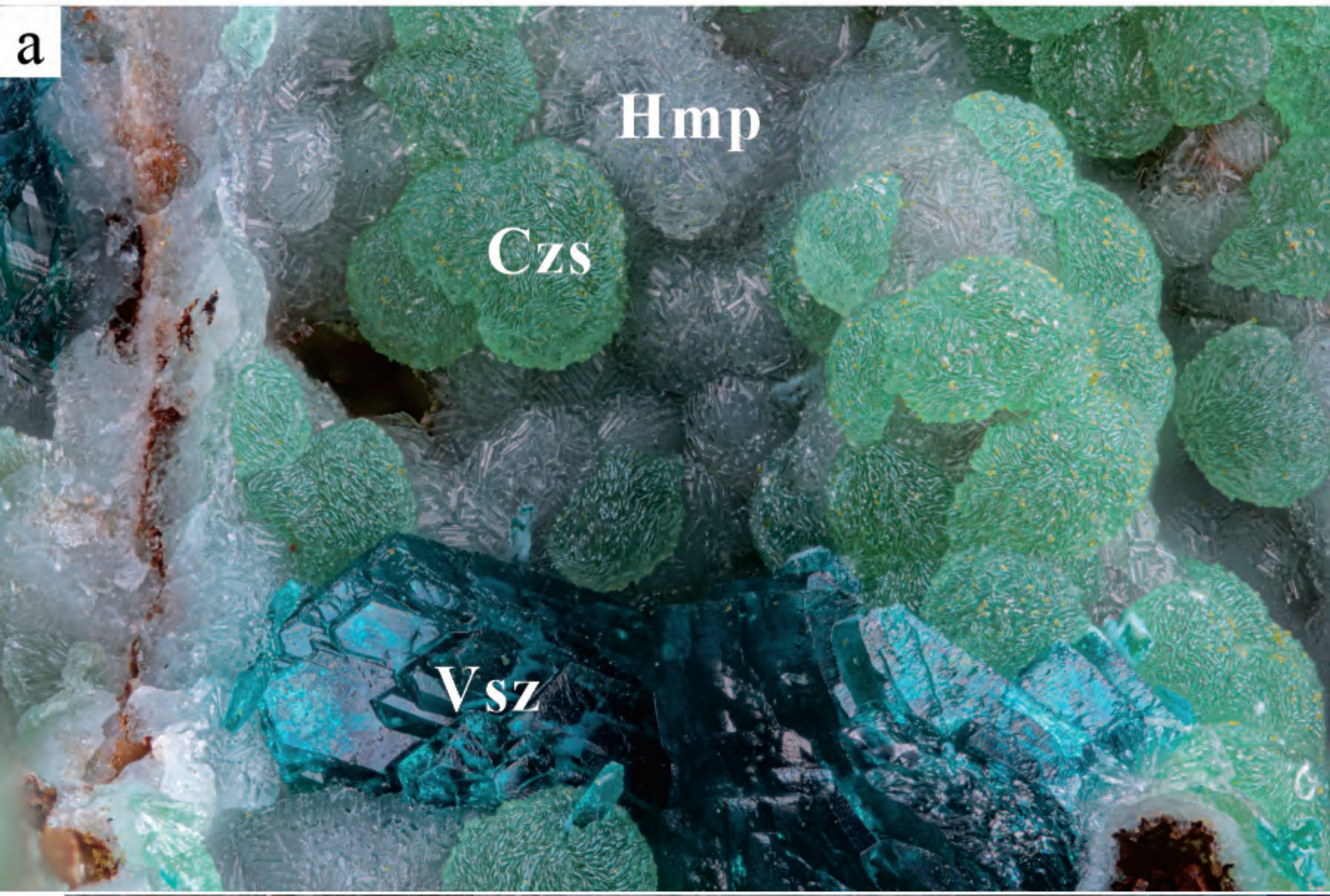

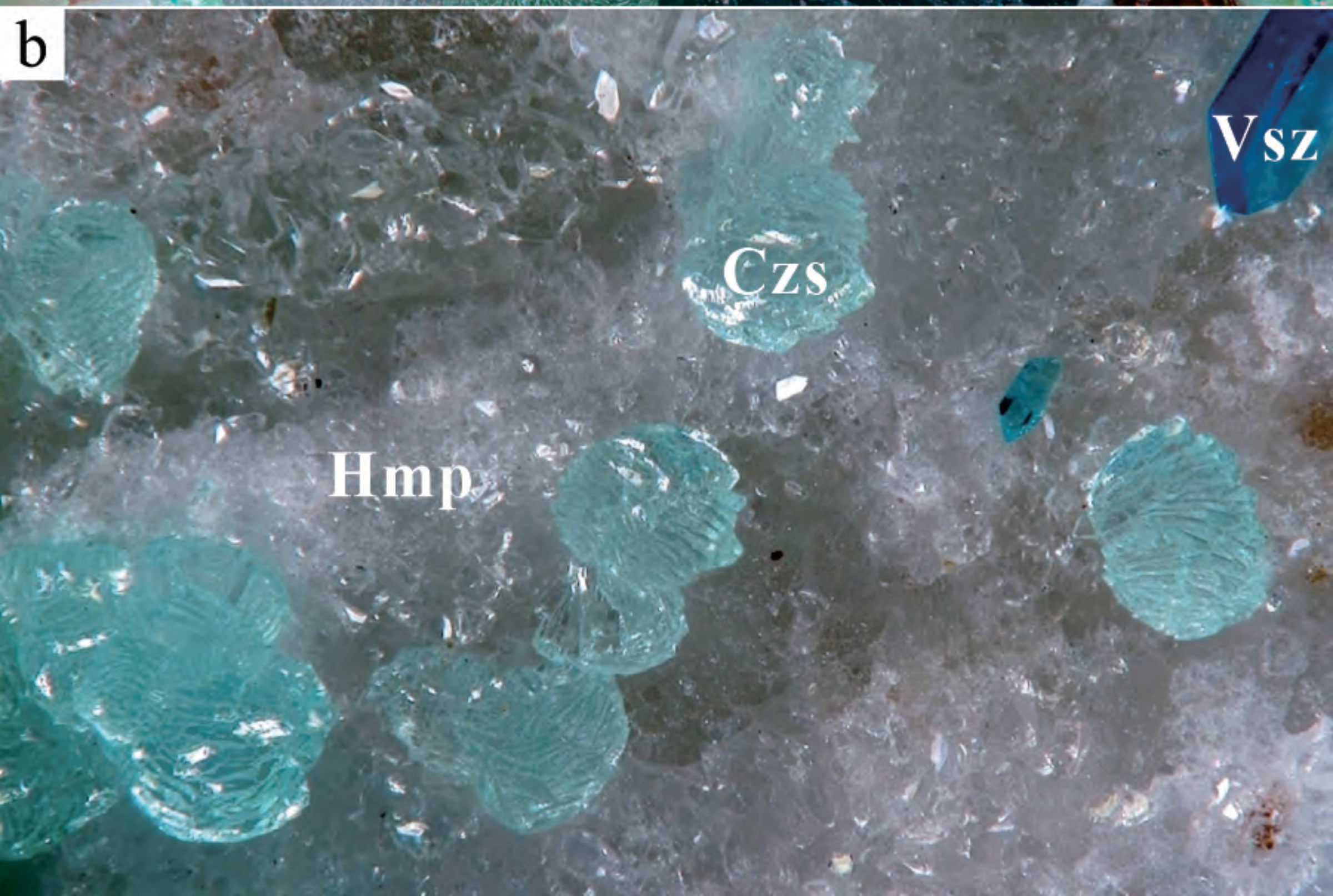

Figure 3

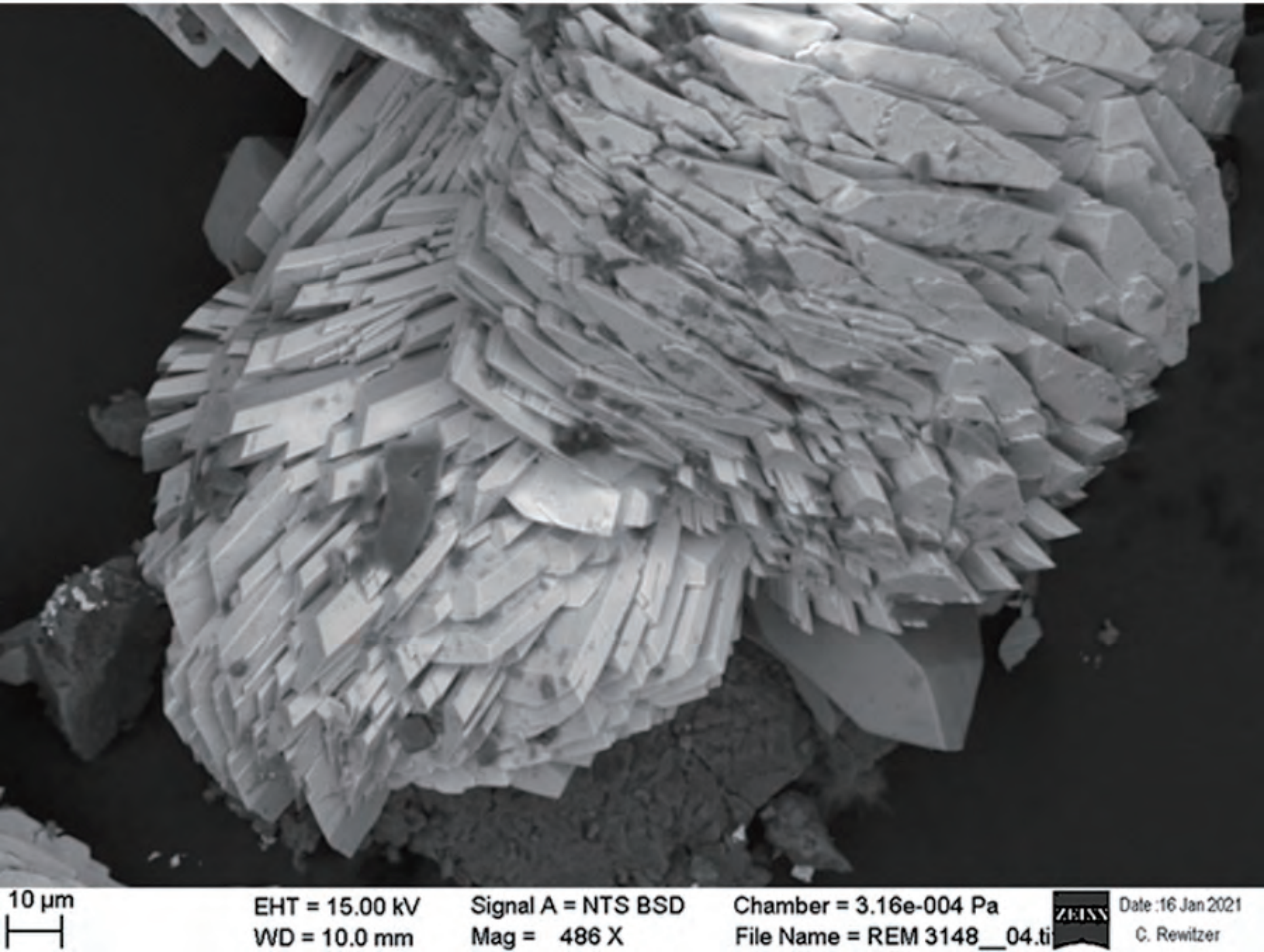
10 µm
EHT = 15.00 kV
WD = 10.0 mm
Signal A = NTS BSD
Mag = 486 X
Chamber = 3.16e-004 Pa
File Name = REM 3148__04.ti
ZEISS
Date :16 Jan 2021
C. Rewitzer

Figure 4

a

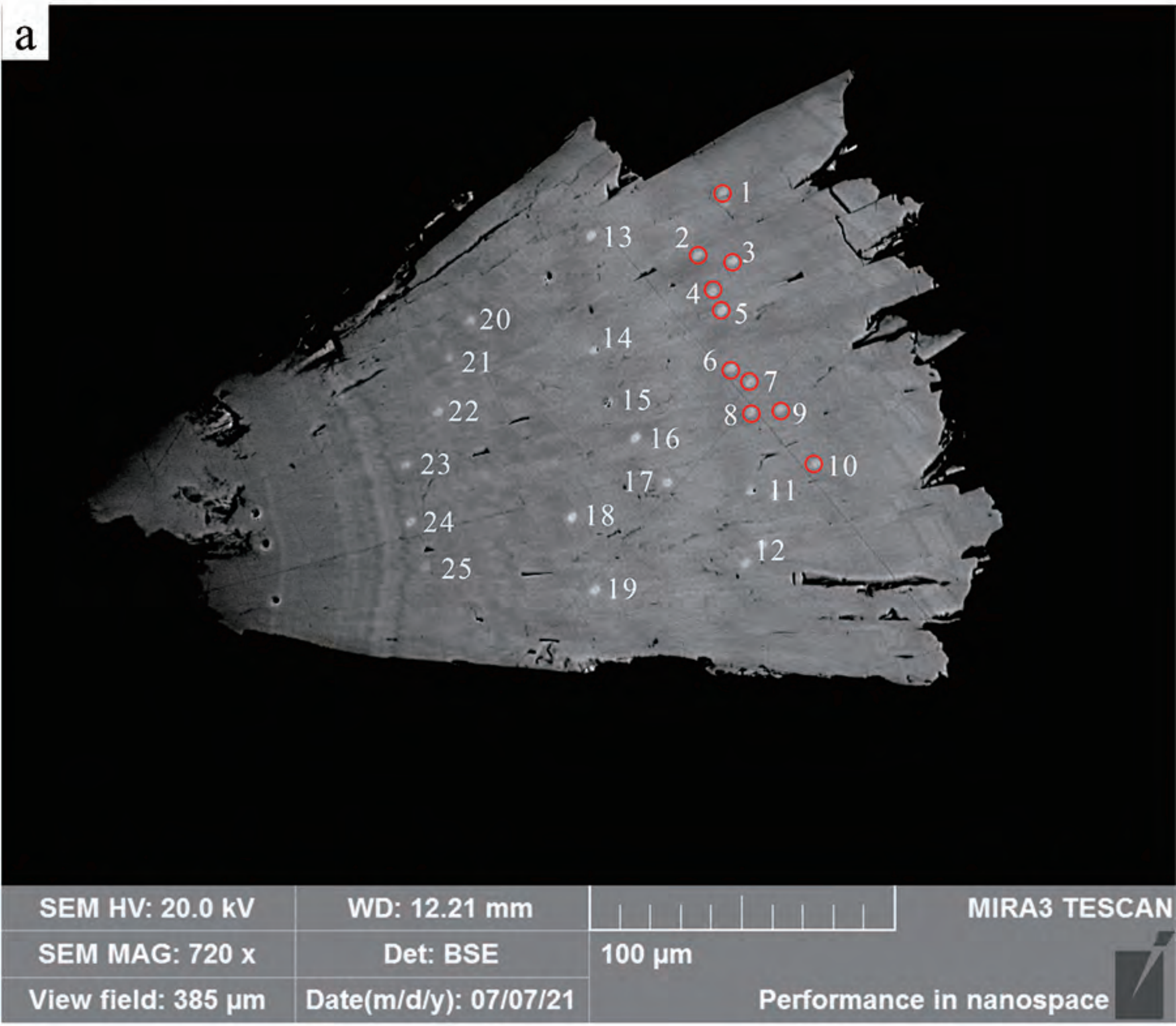
1
2
3
4
5
6
7
8
9
10
11
12
13
14
15
16
17
18
19
20
21
22
23
24
25
SEM HV: 20.0 kV
WD: 12.21 mm
MIRA3 TESCAN
SEM MAG: 720 x
Det: BSE
100 μm
View field: 385 μm
Date(m/d/y): 07/07/21
Performance in nanospace

b

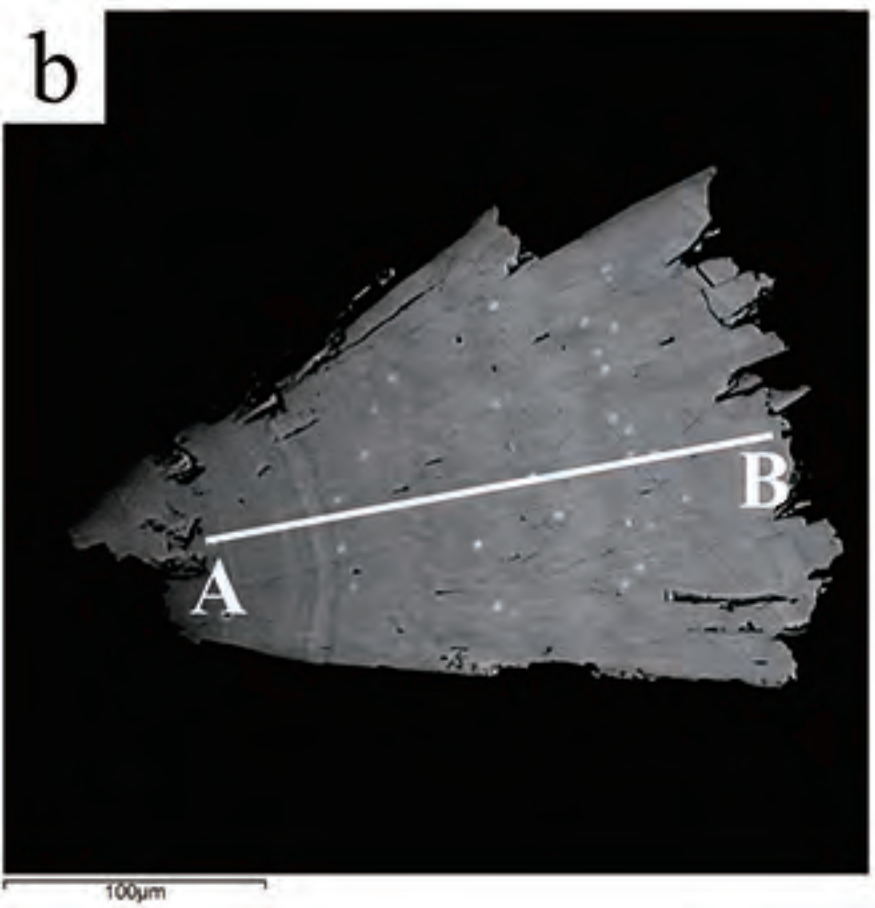
A
B
100μm

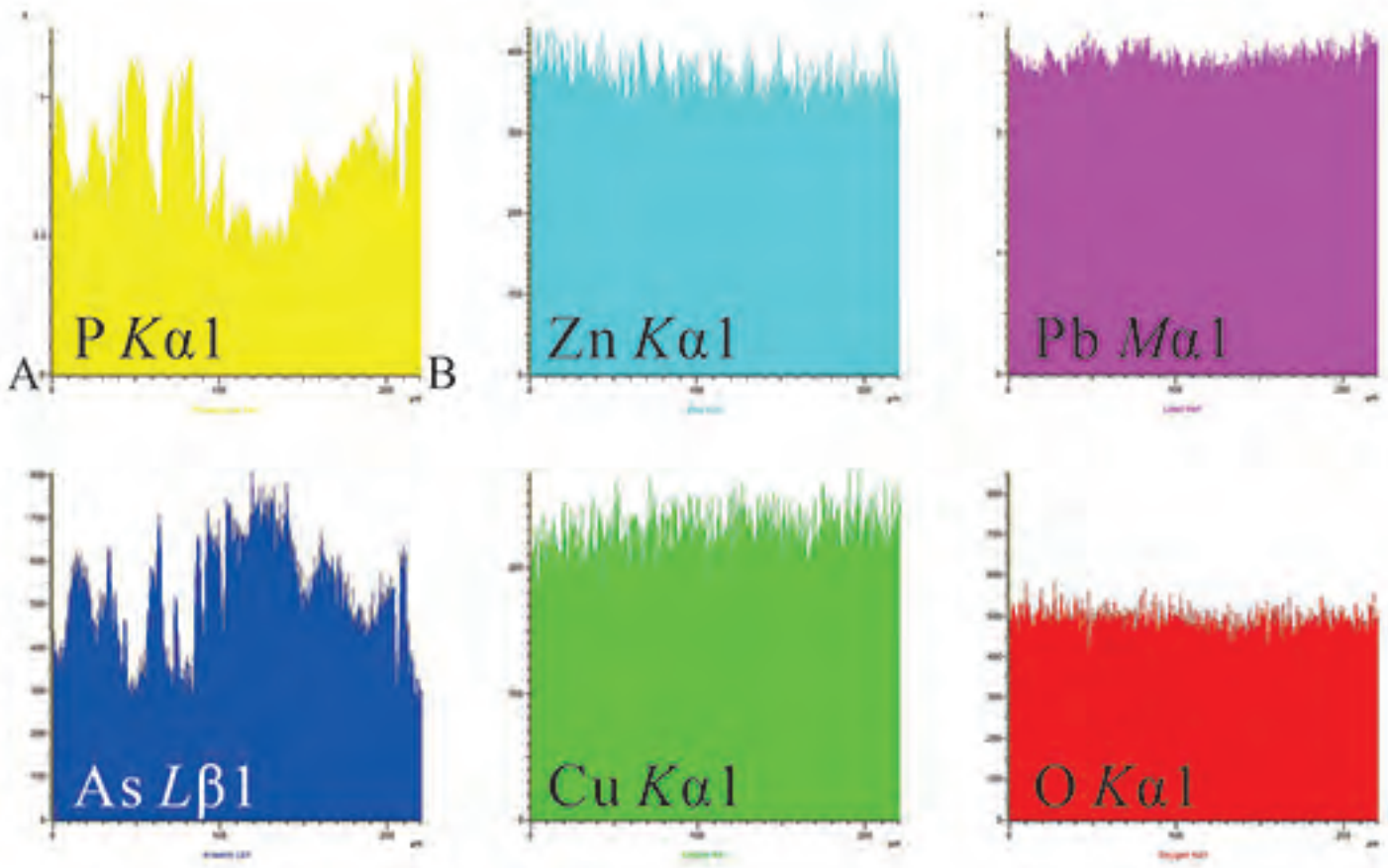
P Kα1
A
B
Zn Kα1
Pb Mα1
As Lβ1
Cu Kα1
O Kα1

Figure 5

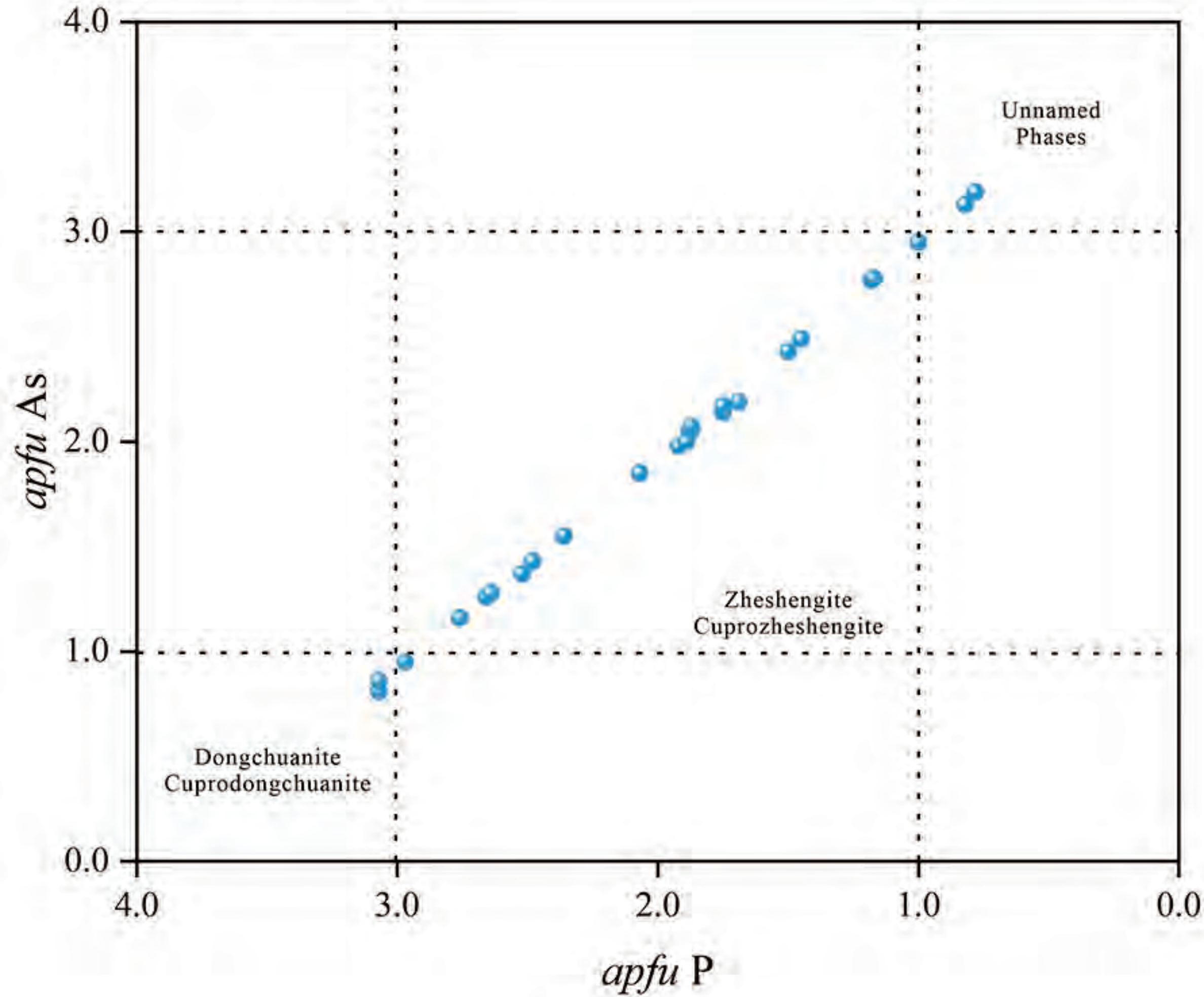
4.0
3.0
2.0
1.0
0.0
apfu As
Unnamed
Phases
Zheshengite
Cuprozheshengite
Dongchuanite
Cuprodongchuanite
4.0
3.0
2.0
1.0
0.0
apfu P

Figure 6

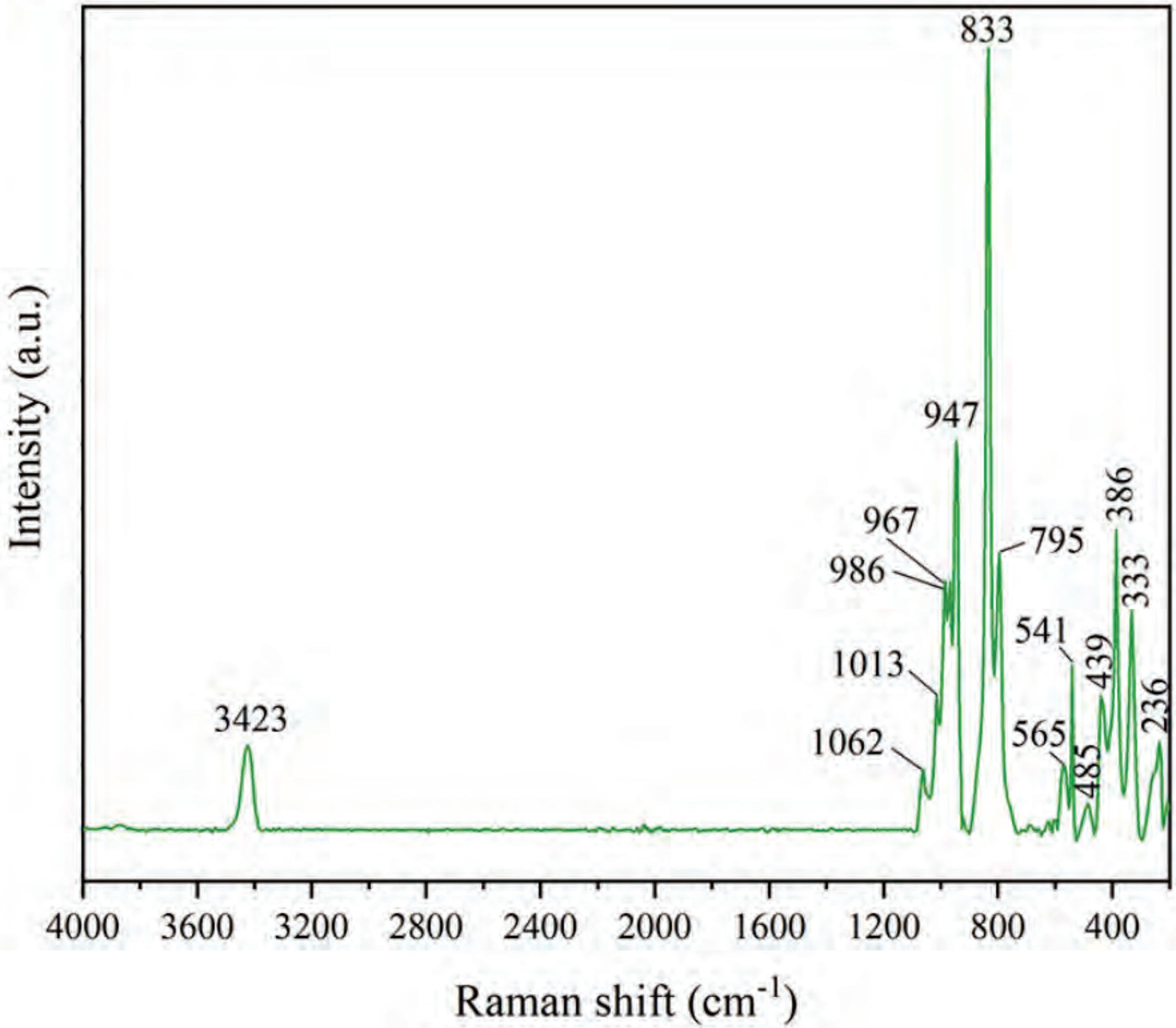
833
947
967
986
795
386
333
541
439
1013
236
3423
1062
565
485
Intensity (a.u.)
4000
3600
3200
2800
2400
2000
1600
1200
800
400
Raman shift (cm-1)

Figure 7

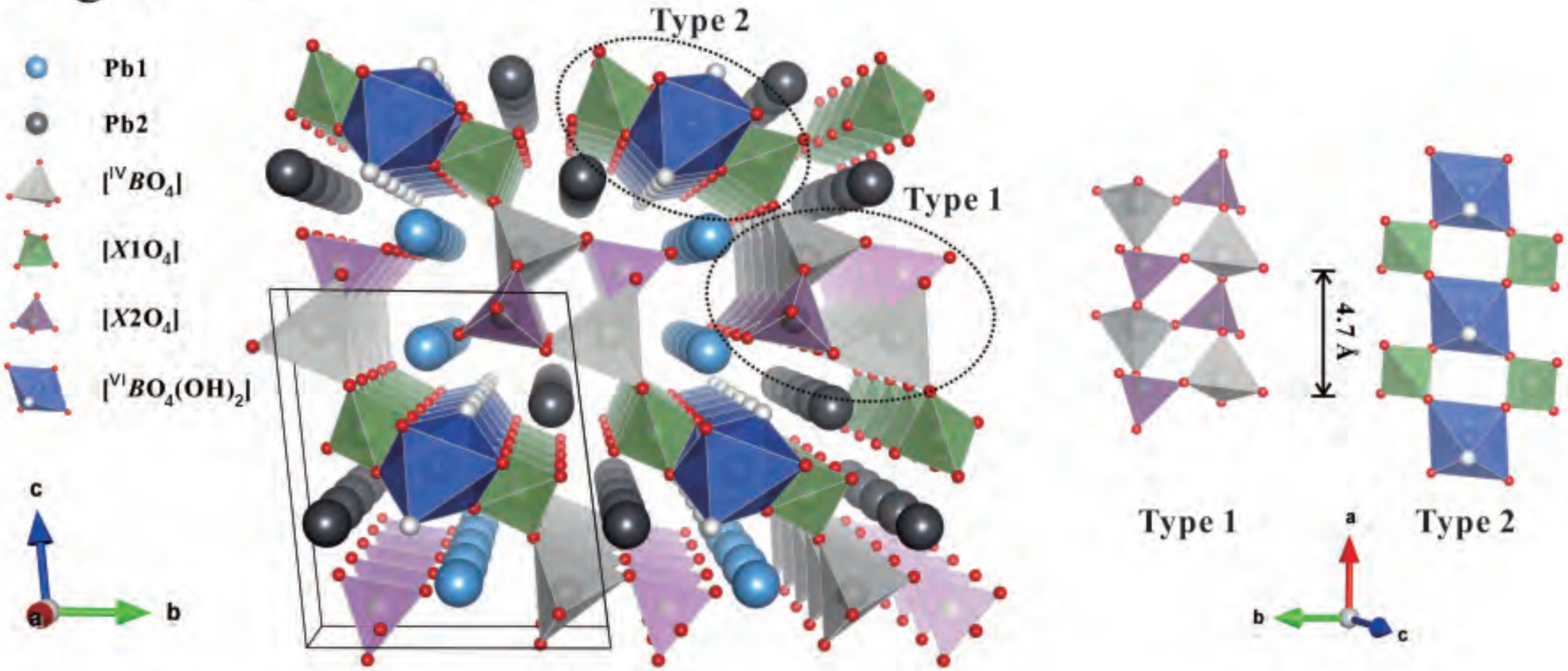
Pb1
Pb2
[$^{IV}BO_4$]
[$X1O_4$]
[$X2O_4$]
[$^{VI}BO_4(OH)_2$]
Type 2
Type 1
c
a
b
4.7 Å
Type 1
Type 2
a
b
c

Figure 8

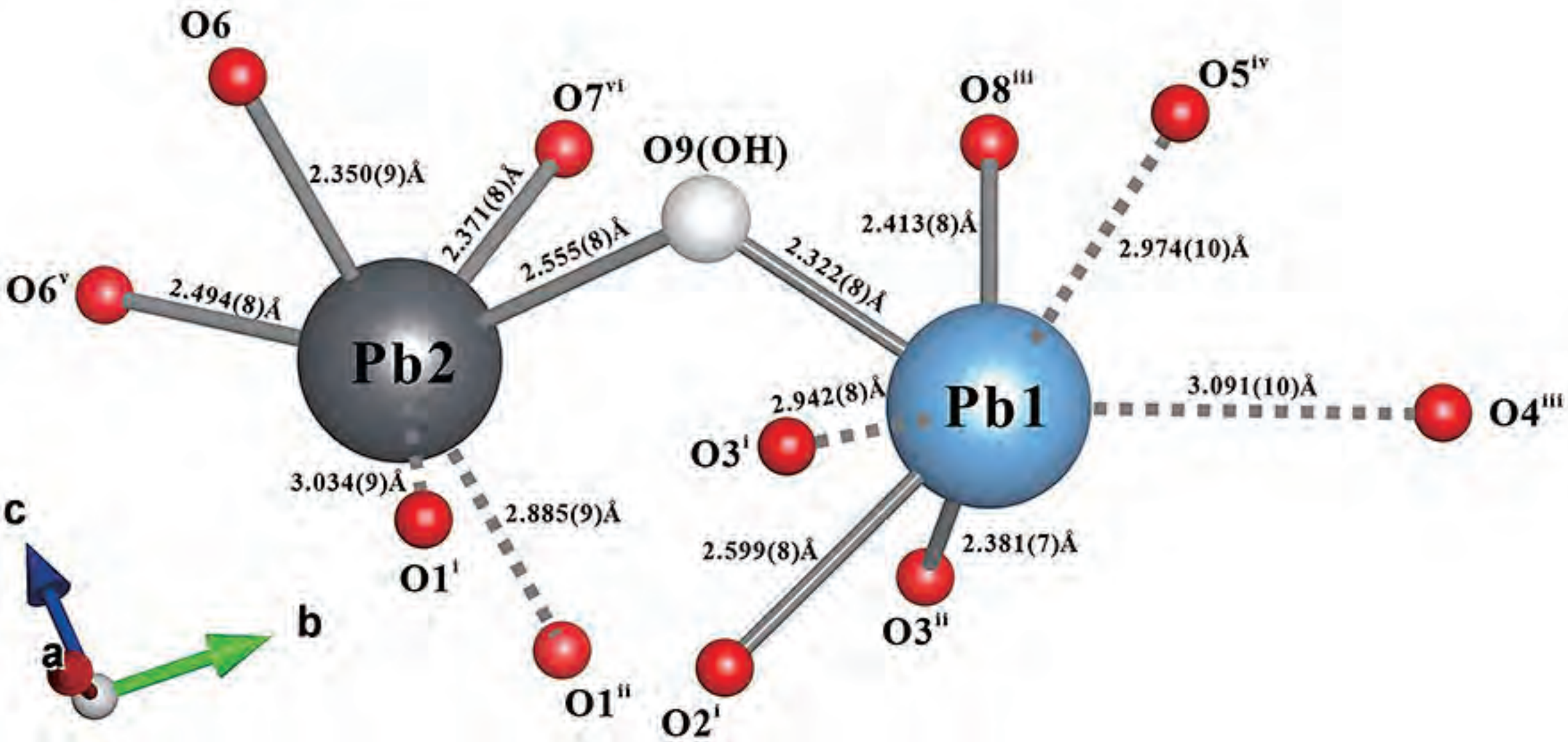
O6
O7vi
O9(OH)
O8iii
O5iv
2.350(9)Å
2.371(8)Å
2.555(8)Å
2.322(8)Å
2.413(8)Å
2.974(10)Å
O6v
2.494(8)Å
Pb2
Pb1
2.942(8)Å
3.091(10)Å
O4iii
O3i
3.034(9)Å
2.885(9)Å
O1i
2.599(8)Å
2.381(7)Å
O3ii
O1ii
O2i
c
b
a

Figure 9

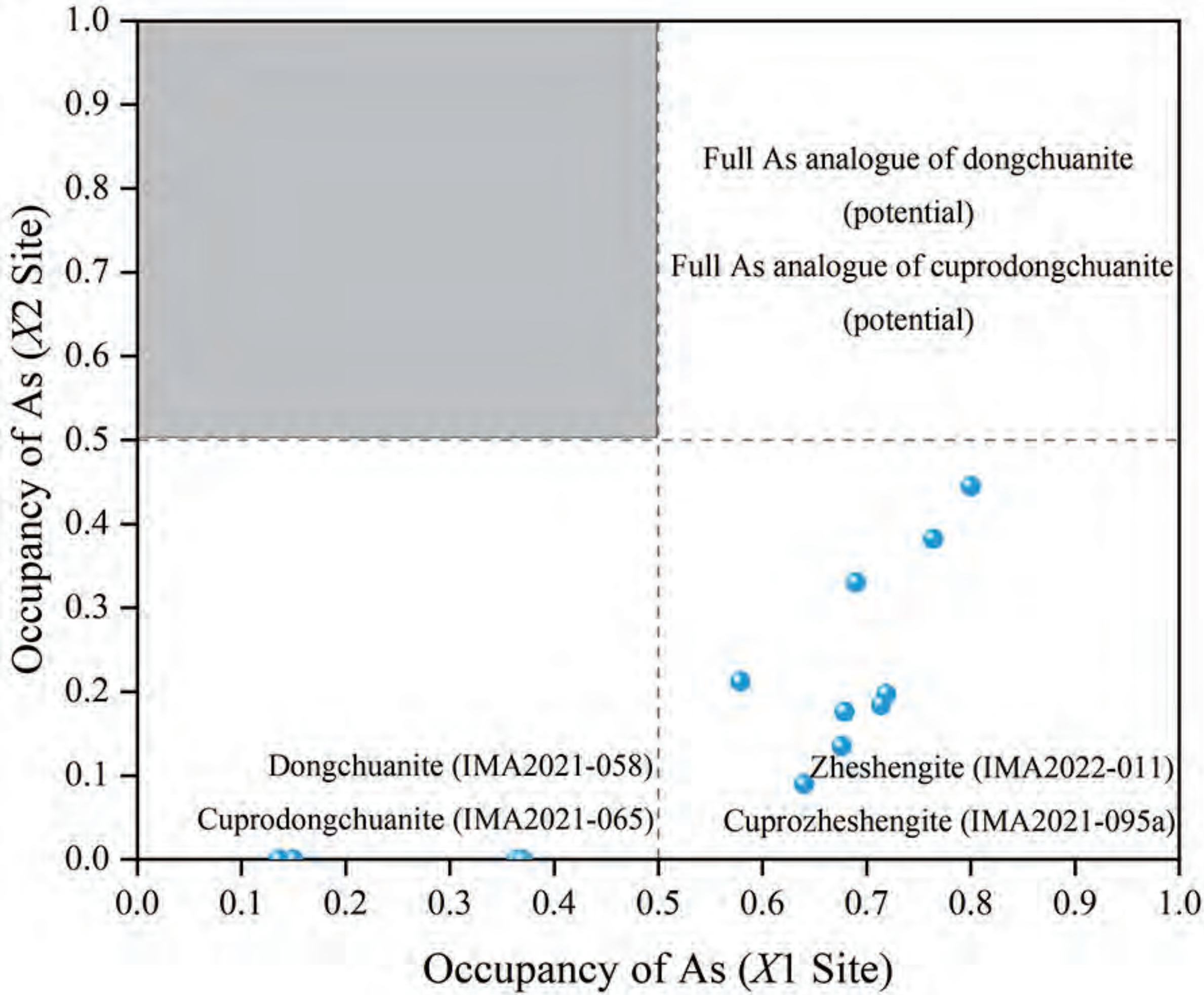
Full As analogue of dongchuanite
(potential)
Full As analogue of cuprodongchuanite
(potential)
Dongchuanite (IMA2021-058)
Cuprodongchuanite (IMA2021-065)
Zheshengite (IMA2022-011)
Cuprozheshengite (IMA2021-095a)
Occupancy of As (X2 Site)
Occupancy of As (X1 Site)
0.0
0.1
0.2
0.3
0.4
0.5
0.6
0.7
0.8
0.9
1.0

Figure 10

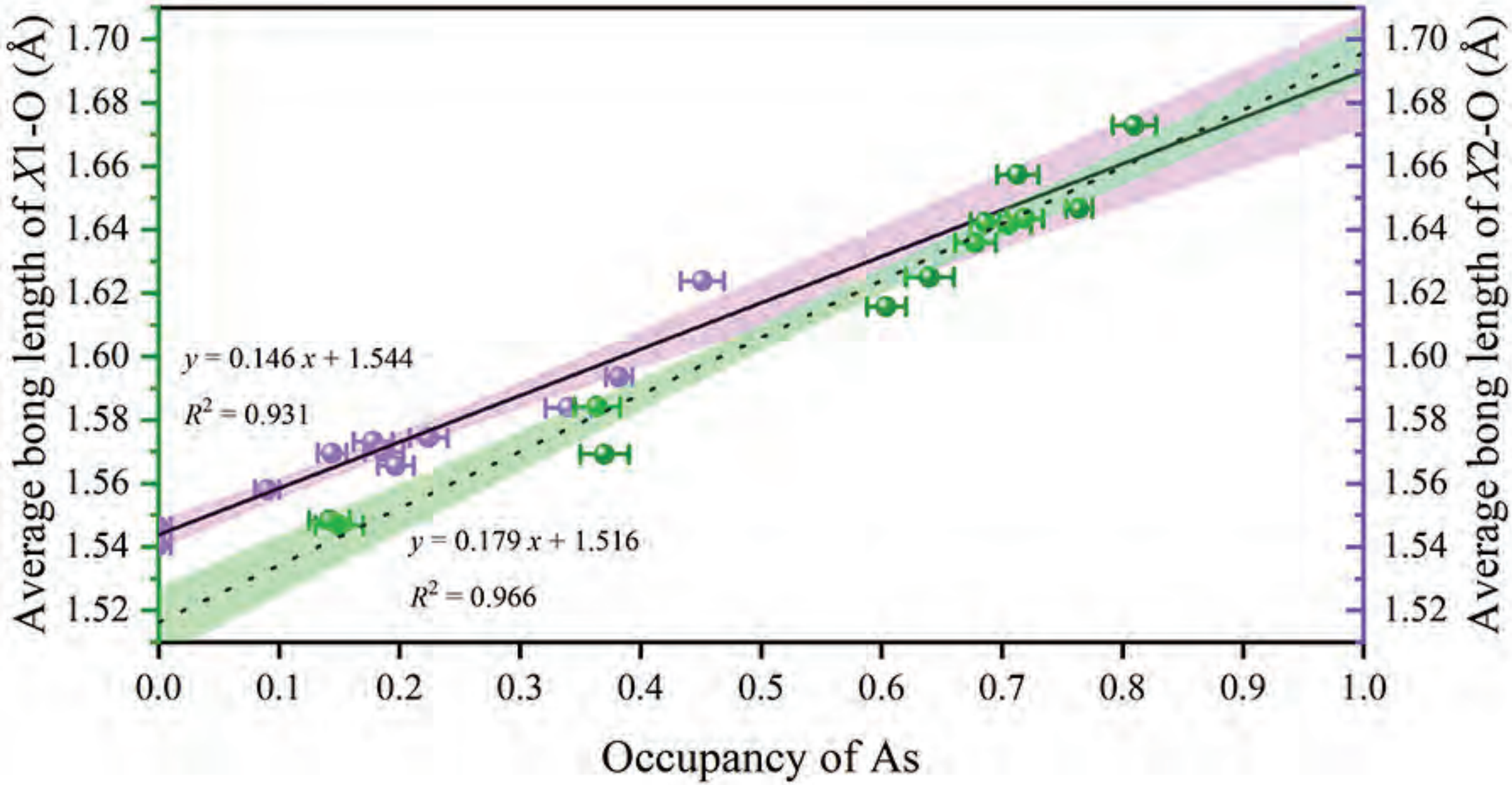
Average bong length of X1-O (Å)
Average bong length of X2-O (Å)
Occupancy of As
y = 0.146 x + 1.544
R² = 0.931
y = 0.179 x + 1.516
R² = 0.966
1.70
1.68
1.66
1.64
1.62
1.60
1.58
1.56
1.54
1.52
0.0
0.1
0.2
0.3
0.4
0.5
0.6
0.7
0.8
0.9
1.0

Figure 11

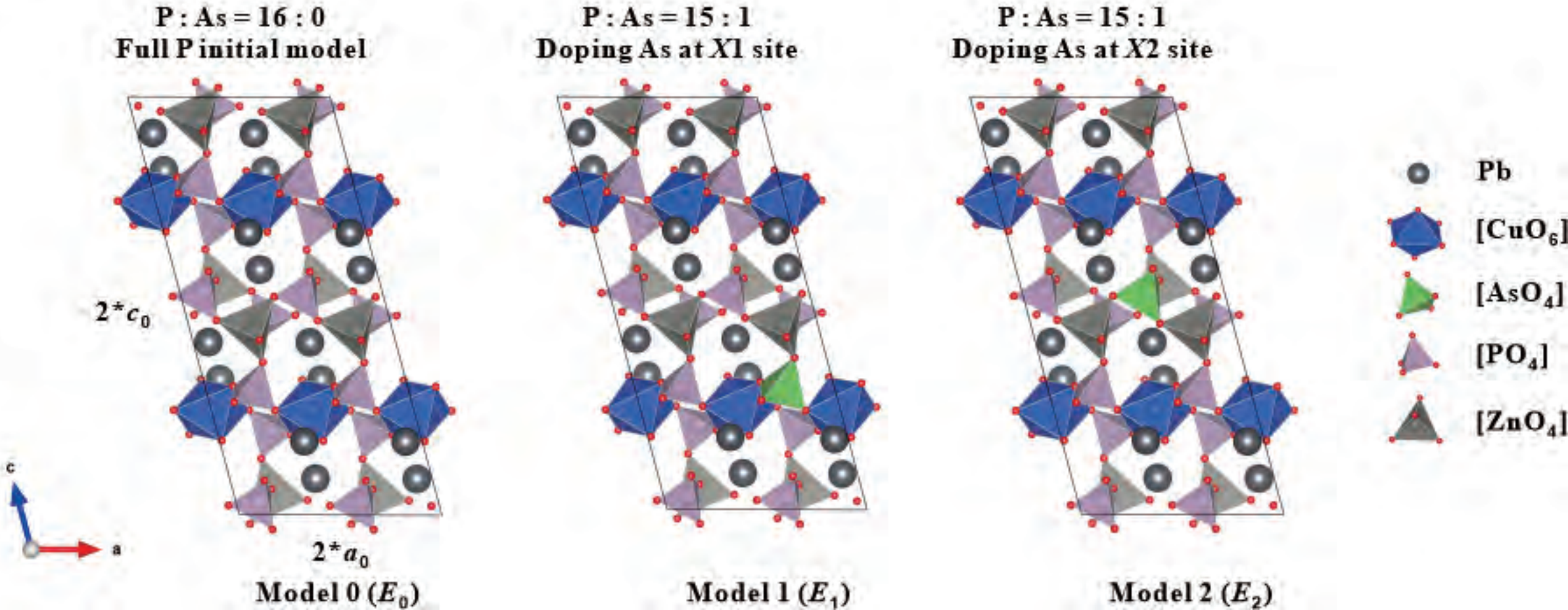
P : As = 16 : 0
Full P initial model
P : As = 15 : 1
Doping As at X1 site
P : As = 15 : 1
Doping As at X2 site
2*c0
2*a0
c
a
Model 0 (E0)
Model 1 (E1)
Model 2 (E2)
Pb
[CuO6]
[AsO4]
[PO4]
[ZnO4]